


2018

Computational Investigation of Protein Assemblies

SM Bargeen Alam Turzo
Cleveland State University

Follow this and additional works at: <https://engagedscholarship.csuohio.edu/etdarchive>

 Part of the [Biochemistry, Biophysics, and Structural Biology Commons](#), and the [Chemistry Commons](#)

How does access to this work benefit you? Let us know!

Recommended Citation

Turzo, SM Bargeen Alam, "Computational Investigation of Protein Assemblies" (2018). *ETD Archive*. 1090.
<https://engagedscholarship.csuohio.edu/etdarchive/1090>

This Thesis is brought to you for free and open access by EngagedScholarship@CSU. It has been accepted for inclusion in ETD Archive by an authorized administrator of EngagedScholarship@CSU. For more information, please contact library.es@csuohio.edu.

COMPUTATIONAL INVESTIGATION OF PROTEIN ASSEMBLIES

SM BARGEEN ALAM TURZO

Bachelor of Arts in Chemistry

Ohio Wesleyan University

May 2016

submitted in partial fulfillment of requirements for the degree

MASTER OF SCIENCE IN CHEMISTRY

at the

CLEVELAND STATE UNIVERSITY

AUGUST 2018

We hereby approve this thesis for

SM BARGEEN ALAM TURZO

Candidate for the Master of Science in Chemistry degree for the

Department of Chemistry

and

CLEVELAND STATE UNIVERSITY'S

College of Graduate Studies by

Thesis Chairperson, Valentin Gogonea
Chemistry Department

Date

Thesis Committee Member, Warren Christopher Boyd
Chemistry Department

Date

Thesis Committee Member, Mekki Bayachou
Chemistry Department

Date

Date of Defense: June 18, 2018

ACKNOWLEDGEMENT

This thesis would have been impossible without the brilliant mind of my advisor Dr. Valentin Gogonea. I joined Dr. Gogonea's lab with a lot of passion and zero expertise in the field, however Dr. Gogonea has helped me develop the necessary skills in this field and made my passion for Computational Chemistry even stronger. His expertise and thorough knowledge in this field has helped me to build the mindset expected from a chemistry graduate students. I am grateful to Dr. Stanley Hazen for allowing me to closely work with his lab members at Lerner Research Institute, Cleveland Clinic Foundation. I would also like to thank my friend Justin Seffernick and Syed Galib Fida Karuni for their help in Python and C++ scripting respectively. Last but not the least, I thank my family for supporting my decision to do graduate studies, for their understanding and patience through some of the most difficult times in this journey and I am indebted forever for their love and support. This work used the Extreme Science and Engineering Discovery Environment (XSEDE), which is supported by National Science Foundation grant number ACI-1548562. I would also especially like to express my gratitude to Dr. Mahidhar Tatineni at the supercomputer center(COMETS DSC) in San Diego for all his help in helping me prepare batch scripts for submitting jobs at the supercomputer center.

COMPUTATIONAL INVESTIGATION OF PROTEIN ASSEMBLIES

SM BARGEEN ALAM TURZO

ABSTRACT

Selective nitrosylation of glyceraldehyde 3-phosphate dehydrogenase (GAPDH) at Cys-247 affects gene regulation through the interferon-gamma (IFN- γ) activated inhibitor of translation (GAIT) complex. Oxidized low-density lipoprotein (LDLox) and INF- γ induce assembly of the nitrosylase complex composed of inducible nitric oxide synthase (iNOS), S100A8, and S100A9 proteins. Crystal structure of the complex of GAPDH and S100A8A9 is not known, structural prediction method were employed by protein-protein docking and binding energy calculation with PatchDock and FIREDock respectively. Candidate models were selected, based on a weight factor calculated, from the computational method developed from the "artificial protease" cleavage mapping Fe(III) (s)-1-(p- bromoacetamidobenzyl) EDTA to identify helical domains of GAPDH that interact with S100A8. Models were also selected based on the Boltzmann distribution according to their binding energy. Interface residue analysis suggest that from the models that matched with experimental data, DCE-9 has highest weight factor of 1.68. Docking complexes without experimental bias has the highest binding energy of -76.04 kcal/mol when compared to other candidate models. Our analysis also suggests that complex that matched with experimental data are less likely to form as their binding energies were much lower when compared to the models that were not selected based on experimental data. It can be inferred from our analysis that artificial cleavage mapping may lead to artefacts and the CHARMM19 force field used in FIREDock may not accurately represent the true binding energy of these complexes.

TABLE OF CONTENTS

	Page
ABSTRACT	iv
LIST OF TABLES	vii
LIST OF FIGURES	viii
LIST OF ABBREVIATIONS	ix
CHAPTER	
I. INTRODUCTION.....	1
II. METHODS.....	4
2.1. Docking Process of S100A8A9 and GAPDH.....	4
2.2. Selection of Models based on experimental results.....	5
2.3. Selection of Models based on Boltzmann Distribution.....	8
2.4. Interface Residues Analysis of Selected Models.....	8
III. RESULTS AND DISCUSSION.....	10
3.1 DCE-9 with Best Weight Factor from Optimization.....	10
3.2. DC-1 as the Best Predicted Structure.....	18
3.3. Interaction Energies of Predicted Complexes.....	22
3.4. Alanine Scanning Results shows Destabilization with Size..	32
3.5. Analysis of the AINT Method.....	35
IV. CONCLUSION.....	37
REFERENCES.....	38
APPENDCIES.....	45
A. Interaction Energies of Interface Residues of all Predicted Models...	45

	Page
B. Virtual Alanine Scanning of all Predicted Models.....	56

LIST OF TABLES

Table		Page
1.	Quantified Results of Experimental Data using ImageJ.....	10
2.	MCs selected using the Accessibility Calculations.....	12
3.	DCs selected using Accessibility Calculations.....	13
4.	TCs selected using Accessibility Calculations.....	14
5.	Candidate Models based on Experimental Match.....	16
6.	Percentage Contribution of Complex to the Quantified Data.....	17
7.	MCs chosen based on Boltzmann Distribution.....	18
8.	DCs chosen based on Boltzmann Distribution.....	19
9.	TCs chosen based on Boltzmann Distribution.....	20
10.	Energies and Distances of Interface Residues of MCE-9 and MC-1...	23
11.	Energies and Distances of Interface Residues of DCE-9 and DC-1...	26
12.	Energies and Distances of Interface Residues of TCE-20 and TC-1...	27

LIST OF FIGURES

Figure		Page
1.	Relative Intensities of GAPDH-S100A8A9 Wildtype and its Mutation.....	11
2.	Models from Quantified Experimental Data and Boltzmann Distribution.....	21
3.	Interface Residue Analysis of MCE-9.....	22
4.	Interface Residue Analysis of MC-1.....	24
5.	Interface Residue Analysis of DCE-9	25
6.	Interface Residue Analysis of DC-1.....	26
7.	Interface Residue Analysis of TCE-20.....	28
8.	Interface Residue Analysis of TC-1.....	28
9.	Interaction Energies of Complex of Monomer GAPDH and S100A8A9.....	29
10.	Interaction Energies of Complex of Dimer GAPDH and S100A8A9.....	29
11.	Interaction Energies of the Complex of Tetramer GAPDH and S100A8A9...	30
12.	Interaction Energies of TCE-15, TCE-18, TCE-19 and TCE-20.....	30
13.	Interaction Energies of MC-1, MC-2 and MC-3.....	31
14.	Interaction Energies of Interface Residues of DC-1, DC-2 and DC-3.....	31
15.	Interaction Energies of Interface Residues of TC-1 and TC-2.....	32
16.	Virtual Alanine Scanning Results of MCE-9 and MC-1.....	33
17.	Virtual Alanine Scanning Results of DCE-9 and DC-1.....	33
18.	Virtual Alanine Scanning Results of TCE-20 and TC-1.....	34

LIST OF ABBREVIATIONS

UTR	Untranslated region
IFN- γ	Interferon-gamma
GAIT	Gamma activated inhibitor of translation
mRNA	messenger Ribonucleic acid
DAPK	Death-associated protein kinase
ZIPK	Zipper-interacting protein kinase
EPRS	glutamyl-prolyl tRNA synthetase
NSAP1	Non structural associated protein 1
NO	Nitric Oxide
SNO	S-nitrosothiol
GAPDH	Glyceraldehyde 3-phosphate dehydrogenase
iNOS	Inducible NO synthase
P-L13a	Phosphorylated large ribosomal protein 13a
S100A8A9	Heterodimer protein consisting of S100A8 and S100A9
EDTA	Ethylenediaminetetraacetic acid
FeBABE	Fe(III) (s)-1-(p-bromoacetamidobenzyl) EDTA
PatchDock	Algorithm for molecular and protein-protein docking
FIREDock	Fast interaction refinement in molecular docking
TAAR	Total accessibility angle of rotation
AINT	Accessibility for an interaction
RAAR	Restricted accessible angle of rotation

$\alpha 1$	Helix 1 of GAPDH
$\alpha 3$	Helix 3 of GAPDH
$C\alpha$	Carbon alpha
RCSB	Research Collaboratory for structural bioinformatics
1XK4	Protein data bank ID for S100A8A9
1ZNQ	Protein data bank ID for tetramer GAPDH
MCE	Monomer GAPDH and S100A8A9 with experimental match
DCE	Dimer GAPDH and S100A8A9 with experimental match
TCE	Tetramer GAPDH and S100A8A9 with experimental match
MC	Monomer GAPDH and S100A8A9 without experimental bias
DC	Dimer GAPDH and S100A8A9 without experimental bias
TC	Tetramer GAPDH and S100A8A9 without experimental bias
$\Delta\Delta G$	Predicted change in binding free energy
WT	Wild type
GROMACS	Groningen machine for chemical simulations
TIP3P	Transferable intermolecular potential with 3 points
CHARMM27	Chemistry at Harvard macromolecular mechanics version 27
PME	Particle mesh Ewald
XSEDE	Extreme science and engineering discovery environment
SDSC	San Diego supercomputer center
PD#	PatchDock number for retrieving the docking complex
BE	Binding Energy of the docking complex
CE	Complex with experimental match

W.F.	Weight factor
p(MC)	Probability of a complex with monomer GAPDH and S100A8A9
p(DC)	Probability of a complex with dimer GAPDH and S100A8A9
p(TC)	Probability of a complex with tetramer GAPDH and S100A8A9
I.E.	Interaction energy
R.I.	Relative Intensities
QMMM	Molecular mechanics simulations combining quantum mechanics

CHAPTER I

INTRODUCTION

Transcript-selective translation inhibition plays a major role in post-transcriptional mechanism to regulate gene expression. This process generally occurs in the 5' and/or 3' untranslated region (UTR) by the binding of a protein complex to a specific sequence or structural elements in the designated UTR [1, 2]. Several studies show that specific post-transcriptional mechanism within the 3'UTR are critical for the regulation of gene expression that are associated with inflammation [3, 4]. The inflammatory cytokine gamma interferon (IFN- γ) in human myeloid cells causes the formation of heterotetrameric, IFN- γ -activated inhibitor of translation (GAIT) complex that binds to specific region of the GAIT element in the 3'UTR to various mRNAs that are responsible for inflammation and inhibits their translation [4]. Vascular endothelial growth factor A, ceruloplasmin, death-associated protein kinases DAPK and ZIPK are some of these mRNAs, whose translation are inhibited [4, 5]. The constituents of the GAIT complex in human are glutamyl-prolyl-tRNA synthetase (EPRS), ribosomal protein L13a, glyceraldehyde-3-phosphate dehydrogenase (GAPDH) and NS1-associated protein 1(NSAP1) [6]. Studies have further suggested that the major function of GAIT complex is to restrict the responsible for restricting the IFN- γ -inducible inflammatory

gene expression, where the major function of the GAIT pathway is to impede the accumulation of excess inflammatory proteins responsible for damaging host tissue and suppress highly stable mRNAs that avoid early transcriptional blocks [4]. Genetic disorder in the components of the GAIT complex has also been suggested to cause excess inflammatory gene expression and could lead to chronic inflammatory disorders and fatal tumor growth [7, 8].

S-Nitrosylation is a covalent attachment of nitric oxide (NO) to a cysteine residue in a protein to form an S-nitrosothiol (SNO) and is a form of (NO)-dependent post-translational modification of cysteine that is important for the structure and function of protein and plays a major role in a various of signaling pathways [9, 10]. While physiological S-nitrosylation is required for proper cellular activity and functions, dysregulation of S-nitrosylation has also been known to lead to severe diseases [11, 12, 13]. Protein S-nitrosylation is also site-selective, regulatable and reversible [14]. Recent studies have also shown that GAPDH, an important enzyme responsible for the breakdown of glucose to produce energy and pyruvic acid in the glycolysis process is a target of S-nitrosylation and its activity affected by S-nitrosylation [15]. In a recent study it was also reported that oxidatively modified low-density lipoprotein subdues the activity of the GAIT system through selective S-nitrosylation of GAPDH at Cys247 [16]. This S-nitrosylation fails to bind and protect the protein L13a and therefore leads to failure in the formation of the GAIT complex [16]. In order for the S-nitrosylation of GAPDH to occur at Cys247, inducible NO synthase (iNOS) is required and the binding of iNOS to GAPDH is bridged by the heterodimeric complex S100A8 and S100A9 (S100A8A9) [14]. S100A8A9 is considered to be a pro-inflammatory agent and are abundantly found

in inflammatory sites [17, 18, 19]. Studies also show that S100A9 of the S100A8A9 heterodimeric complex is specifically required for the S-nitrosylation of GAPDH at Cys 247 and the depletion of this protein restores the activity of the GAIT system. S100A8 is needed for site selectivity of S-nitrosylase complex in GAPDH S-nitrosylation and depletion of S100A9 restores the activity of the GAIT system [14]. Depletion of iNOS and S100A9 have also shown benefits in animal models of Alzheimer's disease [20, 21]. There are also further experimental evidence of the interaction of the wild type S100A8 and its three mutants (I22C, D32C and D52C) with $\alpha 1$ and $\alpha 3$ helices GAPDH using FeBABE (Fe(III) (s)-1-(p-bromoacetamidobenzyl) EDTA) "artificial protease" method [14, 22]. Since the crystal structure of the complex of GAPDH and S100A8A9 is not known, in this study we use protein-protein docking for docking the complex structure of GAPDH and S100A8A9 and developed a virtual artificial protease method to predict possible structures that to help narrow down the complexes that are the most dominant in the binding of this complex.

We also use molecular mechanics to study the interaction energy of the interface residues and use virtual alanine scanning techniques to look at interface residues that causes the most destabilization of the predicted complex.

CHAPTER II

METHODS

The crystal structure of the complex S100A8A9 bound to GAPDH is not known, therefore known crystal structures of S100A8A9 (1XK4) [23] and GAPDH (1ZNQ) [24] were taken from RCSB protein data bank. GAPDH is also known to exist as monomer (chain O), dimer (chain O and P) and tetramer (chain O, P, Q and R) [25, 26], the monomer and the dimer were created accordingly from the crystal structure of the tetramer GAPDH (chain O, P, Q and R).

2.1. Docking Process of S100A8A9 and GAPDH

PatchDock web server [27, 28] was used to for the docking of S100A8A9 and GAPDH. Docking jobs were submitted separately for the monomer, dimer and tetramer of GAPDH with S100A8A9. In the PatchDock server, GAPDH was treated as the receptor molecule and S100A8A9 was treated as the ligand molecule. No binding site information or distance constraint was provided to the program. A total of 17743 complexes were predicted by the PatchDock algorithm for the complex of monomer GAPDH and S100A8A9, 22564 for the dimer GAPDH and S100A8A9 and 22688 for the tetramer GAPDH and S100A8A9. These complexes were further refined with Fast interaction refinement in molecular docking (FIREDock) web server [29, 30]. For the

submission of these jobs to both PatchDock and FIREDock web-server, the recommended instructions for protein-protein docking, provided on the web server, were followed.

2.2. Selection of Models based on Experimental Results

The complex structures, obtained from FIREDock [29, 30], were chosen according to their lowest predicted binding energy score. Complexes with negative binding energies were kept for further analysis and all other docking with positive binding energies were discarded. Based on the experimental protein-protein interaction data of the complex of GAPDH and S100A8A9 [16], a computational method was developed to pick out potential structures from the pool of structures with negative binding. Since PatchDock algorithm does protein-protein docking using shape complementarity principles [27], the computational method developed was also based on the shape, surface and distance cut-offs of the subunits within a given complex. Similar to the artificial protease experiment of GAPDH and S100A8A9 [16], S100A8 of the complexes at positions I12, I22, D32, D52, T62, L72 and A82 were mutated to cysteine. Then the carbon alpha ($C\alpha$) of the iron-(S)-1-[p-(bromoacetamido)benzyl]EDTA (FeBABE arm) [22] was attached to the sulfur atom of at each of these mutated positions. The FeBABE arm as then rotated around this bond to check for the total accessibility angle of rotation (TAAR). Then the FeBABE arm was again rotated to point towards the alpha 1 ($\alpha 1$) and alpha 3 ($\alpha 3$) [24] helix of GAPDH within the complex and a maximum distance of 25Å [22] was used to check for the restricted accessible angle of rotation (RAAR) from the FeBABE arm, attached on the S100A8, to the $\alpha 1$ and then to $\alpha 3$ helix of GAPDH. From this the accessibility for an interaction (AINT) to happen was calculated by Equation 1.

$$AINT = \frac{RAAR}{TAAR}, \text{ while RAAR distance constraint } \leq 25\text{\AA} \quad (1)$$

In order to rule out structures that were not relevant to the experimental data, the FeBABE arm was placed on positions I12, T62, L72 and A82. All structure that had a distance of 25Å or less between the FeBABE arm on S100A8 to the α1 and α3 helices of GAPDH were discarded. Furthermore structures, where the distance was less than equal to 25Å between the FeBABE arm, positioned at C42 of S100A8 and α1 of GAPDH were also discarded. The same was done for D52. Therefore, our accessibility analysis was limited to I22C, D32C of S100A8 with α1 and α3 helices of GAPDH and C42 (WT) and D52C of S100A8 with α3 helix of GAPDH. Using this analysis the search for the complex of S100A8A9-GAPDH was narrowed down to 36 structures for the monomer GAPDH and S100A8A9 complex that matched with experimental data (MCE), 19 structures for the dimer GAPDH and S100A8A9 complex that matched with experimental data (DCE) and 36 structures for the tetramer GAPDH and S100A8A9 complex that matched with the experimental data (TCE). These structures were re-ranked again in FIREDock web server [30], using full refinement level option and increased atomic radius scale from their default 0.8 setting to 0.85, as described in the FIREDock web server, for a final refinement of the selected candidate models. Upon refinement MCE, DCE and TCE went down to 28, 12 and 20 structures from their initial values respectively. It was further hypothesized that the experimental complex that were found upon final refinement were responsible for the bands seen on the experimental data[16]. Therefore, the experimental data was quantified using ImageJ [31], to obtain relative intensities of the α1 and α3 band of each individual mutation compared to its uncut protein. Using the quantified experimental data and the accessibility calculations for all

MCE, DCE and TCE a weight factor was associated for all complex by optimizing Equation 2 while constraining Equation 3, 4, 5, 6 and 7. In the following equations $R.I.^{I22C(\alpha1)}$, $R.I.^{I22C(\alpha3)}$, $R.I.^{D32C(\alpha1)}$, $R.I.^{D32C(\alpha3)}$, $R.I.^{C42(\alpha3)}$ and $R.I.^{D52C(\alpha3)}$ are the relative intensities of each band[16], $AINT_i^{I22C(\alpha1)}$, $AINT_i^{I22C(\alpha3)}$, $AINT_i^{D32C(\alpha1)}$, $AINT_i^{D32C(\alpha3)}$, $AINT_i^{C42(\alpha3)}$ and $AINT_i^{D52C(\alpha3)}$ are the accessibility calculation for each conformer and $W.F._i$ as the variable weight factor for each conformer. The percentage that

$$R.I.^{I22C(\alpha1)} - \sum_{i=1}^{conformers} \left(AINT_i^{I22C(\alpha1)} * W.F._i \right) = 0 \quad (2)$$

$$R.I.^{I22C(\alpha3)} - \sum_{i=1}^{conformers} \left(AINT_i^{I22C(\alpha3)} * W.F._i \right) = 0 \quad (3)$$

$$R.I.^{D32C(\alpha1)} - \sum_{i=1}^{conformers} \left(AINT_i^{I22C(\alpha1)} * W.F._i \right) = 0 \quad (4)$$

$$R.I.^{D32C(\alpha3)} - \sum_{i=1}^{conformers} \left(AINT_i^{I22C(\alpha3)} * W.F._i \right) = 0 \quad (5)$$

$$R.I.^{C42(\alpha3)} - \sum_{i=1}^{conformers} \left(AINT_i^{C42(\alpha3)} * W.F._i \right) = 0 \quad (6)$$

$$R.I.^{D52C(\alpha3)} - \sum_{i=1}^{conformers} \left(AINT_i^{D52C(\alpha3)} * W.F._i \right) = 0 \quad (7)$$

contributes to the band by each structure were also calculated using the relative intensity bands and the new weighted accessibility. Any structure that had a weight factor of 0 were discarded. From this analysis we decreased our search to 6, 4, and 10 structures for MCE, DCE and TCE respectively.

2.3. Selection of Models based on Boltzmann Distribution

Protein are known for their highly dynamic nature and artificially attaching the FeBABE arm using the artificial protease method in an experiment can cause structural deformation of the protein and this in turn may cause artefact in protein-protein interactions experimentally. Therefore the true structure may not be what the experimental data may present. In order to answer this question, the protein structure that PatchDock [27, 28] and FIREDock [29, 30] algorithm ranked as the best dockings where also sampled using Boltzmann population analysis as shown in Equation 8, where $p(i)$ is the probability of each structure based on their binding energy, B.E and k is the Boltzmann constant and T is temperature at 273K. From this analysis 3 structures for the

$$p(i) = \frac{e^{\frac{-B.E.}{kT}}}{\sum_{i=1}^{Conformer} e^{\frac{-B.E.}{kT}}} \quad (8)$$

monomer complex (MC) and 3 for the dimer complex (DC) and 2 structures for the tetramer complex (TC) were obtained.

2.4. Interface Residues Analysis of Selected Models

All candidate models, both experimentally biased and unbiased models were subjected to further analysis through a series of investigation of the interface residues. In order to identify the interface residues for each model candidates, ContPro web server [32] was used. The search for interface residue were limited to 5Å between the two subunits of every complex. The shortest distance between the two binding subunits of the candidate models were also obtained. The interface residues obtained for each candidate were further analyzed with virtual alanine scanning using Robetta web server [33] to obtain the predicted change in binding free energy ($\Delta\Delta G$) upon alanine mutation

of each individual mutation, where a positive $\Delta\Delta G$ meant the destabilization of the complex upon mutation of individual residues at the interface to an alanine. Short-range non-bonded interactions between each interface residue and its opposing binding subunit were also calculated in GROMACS2016 [34, 35, 36, 37, 38, 39, 40, 41] by first solvating the complexes with TIP3P water model [42] and by adding NaCl counter ions to neutralize the overall charge of the system. The complexes were then energy minimized with steepest decent algorithm and with periodic boundary conditions in all directions with CHARMM27 Force Field [43, 44] until each complex converged to a local minima. A cut-off distance of 9.0Å was used for the short-range electrostatics and van der Waals interactions. Particle-mesh Ewald (PME) [45] method was used for the treatment of long range electrostatic interactions. A single point energy calculation was done on the energy minimized structure using plain cut-off for electrostatics and van der Waals interactions with no distance cut-offs and no periodic boundary conditions to obtain the full non-bonded short-range interaction energies between a residue and its opposing binding subunit. All computational calculations were performed with supercomputer allocations from XSEDE [46].

CHATER III

RESULTS AND DISCUSSION

3.1 DCE-9 with Best Weight Factor from Optimization

When the experimental data [16] was quantified using ImageJ [31] it was seen that, in case of the wild type (WT) the uncut protein had a 69.63% intensity area and 30.37% when the $\alpha 3$ helix of the GAPDH was cut by the wild type S100A8A9. R.I. of $\alpha 1$ and $\alpha 3$ of GAPDH to I22C, D32C and D52C of S100A8A9 were also calculated from this analysis as shown in Table 1. From the results in Table 1, it is seen that after the

Table 1. The relative intensity for the peaks of $\alpha 1$ and $\alpha 3$ compared to the uncut protein in each case shows consistency with the experimental data [16]

S100A8A9	GAPDH	R.I.
WT(C42)	Uncut	1.00
	$\alpha 3$	0.44
I22C	Uncut	1.00
	$\alpha 3$	0.38
	$\alpha 1$	0.15
D32C	Uncut	1.00
	$\alpha 3$	0.58
	$\alpha 1$	0.75
D52C	Uncut	1.00
	$\alpha 3$	0.42

quantification of the experimental data, when I22 on S100A8 is mutated to a cysteine, then the R.I. is 0.38 for $\alpha 3$ and 0.15 for $\alpha 1$, when compared to the uncut protein. When D32

is mutated to cysteine, then interaction with $\alpha 3$ and $\alpha 1$ were reversed and the relative intensity of $\alpha 1$ was 0.75 and 0.58 for $\alpha 3$. In the case of the mutation of D52 to cysteine and in the case of the wildtype (WT) which is C42, there were similar relative intensities of 0.42 and 0.44 for $\alpha 3$ when compared to the uncut protein. These results were also consistent with the experimental data [16] as shown in Figure 1. The accessibility calculations of the FeBABE arm from these mutated positions of S100A8 was calculated using Equation 1 and the candidate models that were obtained for the complex of monomer GAPDH with S100A8A9 are shown in Table 2.

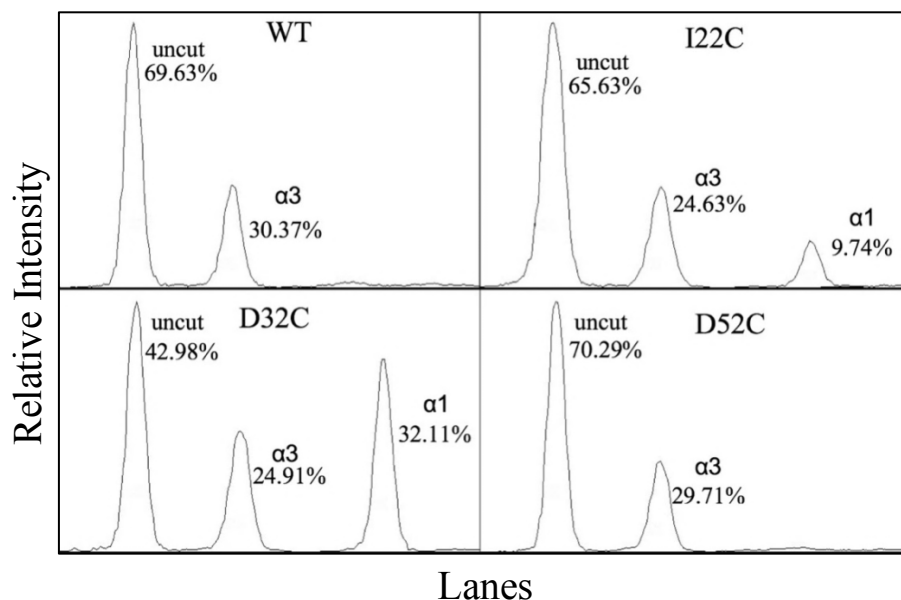


Figure 1. The quantification of experimental data [16] was done by using ImageJ [31] and the intensity of the bands for the wild type (WT), mutation of isoleucine to cysteine at position 22 (I22C), mutation of aspartic acid to cysteine at position 32 (D32C) and at position 52 (D52C) on S100A8A9.

According to the results from Table 2 it is seen that MCE-1 has the best binding energy of -62.75 kcal/mol, however the AINT only shows a partial match with experimental data, where the FeBABE arm on D32C and D52C has AINT to the $\alpha 3$ domain of the monomer GAPDH. These AINT of the FeBABE arm from the mutated positions of

Table 2. Selected Monomer complex obtained from the PatchDock that matched with the experimental data, using the accessibility calculations, are categorized based on their binding energy obtained from FireDock.^a

MCE	PD#	BE	I22C		D32C		C42	D52C
			$\alpha 1$	$\alpha 3$	$\alpha 1$	$\alpha 3$	$\alpha 3$	$\alpha 3$
MCE-1	16032	-62.75	0.00	0.00	0.00	0.30	0.00	0.43
MCE-2	1715	-60.31	0.00	0.00	0.00	0.00	0.00	0.57
MCE-3	1650	-59.47	0.00	0.00	0.00	0.00	0.00	0.23
MCE-4	3030	-56.87	0.00	0.00	0.00	0.00	0.00	0.45
MCE-5	4262	-56.62	0.00	0.00	0.00	0.00	0.00	0.47
MCE-6	10858	-44.18	0.00	0.00	0.00	0.23	0.00	0.44
MCE-7	3785	-40.74	0.00	0.58	0.00	0.36	0.00	0.00
MCE-8	8203	-40.21	0.00	0.25	0.00	0.16	0.00	0.20
MCE-9	8506	-36.82	0.00	0.00	0.00	0.00	0.00	0.22
MCE-10	283	-34.61	0.00	0.00	0.00	0.14	0.34	0.29
MCE-11	7515	-33.00	0.00	0.21	0.00	0.34	0.00	0.00
MCE-12	9998	-32.86	0.00	0.00	0.00	0.21	0.00	0.26
MCE-13	16377	-31.45	0.00	0.00	0.00	0.21	0.00	0.26
MCE-14	11645	-31.36	0.00	0.47	0.00	0.38	0.00	0.32
MCE-15	8027	-27.71	0.00	0.00	0.00	0.00	0.00	0.29
MCE-16	16320	-25.82	0.00	0.00	0.17	0.39	0.00	0.24
MCE-17	62	-24.48	0.00	0.00	0.00	0.27	0.00	0.24
MCE-18	11678	-23.14	0.00	0.00	0.00	0.31	0.00	0.33
MCE-19	11620	-20.77	0.00	0.59	0.00	0.27	0.00	0.19
MCE-20	17163	-20.22	0.00	0.00	0.00	0.47	0.00	0.13
MCE-21	6813	-19.64	0.00	0.51	0.00	0.42	0.00	0.00
MCE-22	15	-16.91	0.00	0.21	0.00	0.19	0.00	0.31
MCE-23	6239	-16.07	0.00	0.00	0.00	0.26	0.00	0.23
MCE-24	3020	-15.83	0.00	0.00	0.00	0.15	0.00	0.26
MCE-25	2100	-12.76	0.00	0.35	0.00	0.22	0.00	0.00
MCE-26	7785	-10.86	0.00	0.28	0.00	0.23	0.00	0.15
MCE-27	11069	-8.36	0.00	0.00	0.00	0.00	0.00	0.49
MCE-28	10277	-7.06	0.00	0.00	0.00	0.51	0.00	0.21

^a I22C, D32C and D52C are the residues on S100A8 that has been mutated to cysteine and WT (C42) is the wild-type of S100A8A9 with no mutations. MCE is the docking of Monomer GAPDH with S100A8A9 that matched with experimental data [16]. PD# is the PatchDock ID with which the structures can be retrieved. BE is the binding energy for the docking GAPDH and S100A8A9 in kcal/mol. $\alpha 1$ and $\alpha 3$ are the domains of GAPDH.

S100A8 to the domains $\alpha 1$ and $\alpha 3$ of GAPDH increases in the case where dimer GAPDH is docked to S100A8A9 as shown in Table 3, DCE-1 has the best binding

Table 3. Selected dimer complex obtained from the PatchDock that matched with the experimental data, using the accessibility calculations, are categorized based on their binding energy obtained from FireDock.^b

			I22C		D32C		C42	D52C
DCE	PD#	BE	$\alpha 1$	$\alpha 3$	$\alpha 1$	$\alpha 3$	$\alpha 3$	$\alpha 3$
DCE-1	4986	-36.48	0.00	0.24	0.00	0.38	0.00	0.26
DCE-2	12596	-33.95	0.00	0.35	0.00	0.24	0.00	0.00
DCE-3	13208	-33.00	0.00	0.23	0.00	0.23	0.00	0.29
DCE-4	16187	-29.05	0.00	0.00	0.00	0.18	0.00	0.00
DCE-5	10038	-27.28	0.00	0.15	0.00	0.40	0.16	0.17
DCE-6	11492	-26.47	0.00	0.25	0.00	0.26	0.00	0.33
DCE-7	1847	-25.00	0.00	0.00	0.00	0.00	0.00	0.10
DCE-8	14710	-16.79	0.00	0.38	0.00	0.39	0.00	0.43
DCE-9	17505	-15.06	0.00	0.00	0.30	0.00	0.00	0.00
DCE-10	14350	-9.25	0.35	0.15	0.31	0.18	0.00	0.28
DCE-11	8026	-3.74	0.00	0.00	0.00	0.12	0.00	0.17
DCE-12	10148	-0.53	0.00	0.15	0.00	0.40	0.16	0.17

^b DCE is the dimer GAPDH docked to S100A8A9 that matched with experimental data. For explanations of other columns in this Table see footnote of Table 2.

energy of -36.48 kcal. AINT calculations also show that FeBABE arm on top of having accessibility to the $\alpha 3$ domain of the dimer GAPDH from D32C and D52C also has accessibility from I22C to $\alpha 3$. The docking complex of tetramer GAPDH and S100A8A9, TCE-1, with a binding energy of -31.48 kcal/mol has FeBABE arm AINT from I22C on S100A8 to both $\alpha 1$ and $\alpha 3$ domain of tetramer GAPDH, D32C on S100A8 to $\alpha 1$ domain of tetramer GAPDH and D52C on S100A8 to $\alpha 3$ domain of tetramer GAPDH as shown in Table 4. Only MCE-10, DCE-5, DCE-12, TCE-4, TCE-9, TCE-17 and TCE-18 were observed were the FeBABE arm had accessibility from the wildtype

(C42) S100A8 to $\alpha 3$ domain of GAPDH. It was also observed from Table 2, 3 and 4 that MCEs had higher binding energies than DCEs and DCEs have higher binding

Table 4. Selected tetramer complex obtained from the PatchDock that matched with the experimental data (TCE), using the accessibility calculations, are categorized based on their binding energy (BE) obtained from FireDock.

			I22C		D32C		C42	D52C
TCE#	PD#	BE	$\alpha 1$	$\alpha 3$	$\alpha 1$	$\alpha 3$	$\alpha 3$	$\alpha 3$
TCE-1	7429	-31.48	0.16	0.14	0.14	0.00	0.00	0.19
TCE-2	5545	-27.90	0.00	0.00	0.00	0.39	0.00	0.23
TCE-3	15335	-24.62	0.12	0.32	0.00	0.00	0.00	0.00
TCE-4	15578	-21.98	0.00	0.00	0.00	0.18	0.63	0.18
TCE-5	1670	-21.09	0.00	0.00	0.00	0.29	0.00	0.28
TCE-6	10862	-20.24	0.00	0.00	0.00	0.18	0.00	0.26
TCE-7	18046	-20.16	0.16	0.27	0.15	0.11	0.00	0.00
TCE-8	7851	-19.76	0.00	0.00	0.00	0.48	0.00	0.20
TCE-9	9943	-17.41	0.00	0.00	0.00	0.00	0.40	0.20
TCE-10	9176	-15.72	0.15	0.16	0.00	0.20	0.00	0.00
TCE-11	22028	-14.27	0.20	0.33	0.00	0.24	0.00	0.21
TCE-12	11963	-11.39	0.36	0.28	0.33	0.19	0.00	0.00
TCE-13	11104	-11.30	0.00	0.00	0.00	0.00	0.00	0.58
TCE-14	876	-9.87	0.00	0.00	0.19	0.18	0.00	0.38
TCE-15	15622	-9.51	0.00	0.00	0.00	0.00	0.00	0.26
TCE-16	15889	-9.50	0.00	0.21	0.00	0.31	0.00	0.12
TCE-17	21611	-8.01	0.00	0.00	0.00	0.31	0.31	0.37
TCE-18	22610	-3.54	0.00	0.00	0.00	0.20	0.43	0.00
TCE-19	110	-2.57	0.00	0.33	0.00	0.00	0.00	0.00
TCE-20	4469	-2.06	0.00	0.00	0.29	0.21	0.00	0.00

^c TCE is the tetramer GAPDH docked to S100A8A9 that matched with experimental data. For explanations of other column see footnote of Table 2.

energies than TCEs. One possible reasoning for this is that complexes formed from monomer GAPDH are more stable and have more geometric features to accommodate binding of S100A8A9 than dimer and Tetramer GAPDH. The AINT increases from MCEs to TCEs is because in the dimer there are two $\alpha 1$ and $\alpha 3$ regions on GAPDH and

in tetramer there are four more regions of $\alpha 1$ and $\alpha 3$. Therefore the FeBABE arm for these dockings have more accessibility to $\alpha 1$ and $\alpha 3$ regions of GAPDH. It also noted that in almost all the cases if there were AINT for the mutations then there were almost no AINT for the C42 the wild type. This is consistent with the experimental data [16]. There were a total of 60 structures observed from Table 2, 3 and 4, to partially match with experimental data, weight factors were calculated for all these candidate models based on the AINT results of these complexes and the R.I.s obtained by minimizing Equation 2 such that Equation 3, 4, 5, 6 and 7 were also minimized. These results presented in Table 5 are independent of binding energies and it is also observed that DCE-9, MCE9 and TCE-20 have a weight factor of 0.32, 1.68 and 0.59 respectively are the highest weighted factor associated among their categories. Based on the weight factors the percentage accessibility of the FeBABE arm from S100A8 to the $\alpha 1$ and $\alpha 3$ were also calculated as shown in Table 6, from these result is seen that DCE-9 which has the highest W.F. also has the highest percentage contribution to R.I.^{D32C($\alpha 1$)}. Results in Table 6 also show that only TCE-4, TCE-9 and TCE-18 have accessibility results for C42 on S100A8. Based on the results of Table 6, the candidate models that were chosen for further analysis were MCE-3, 7, 9, 11, 15 and 21, DCE-4, 7, 9 and 11, TCE-3, 4, 7, 9, 10, 12, 15, 18, 19 and 20. DCE-2 was omitted because of these complexes had extremely low percentage contribution to the accessibility calculations.

Table 5. Weight factors of all the selected complexes that matched with experimental data obtained from the constraint Equation 2.^d

CE	W.F.	CE	W.F.
MCE-1	0.00	DCE-3	0.00
MCE-2	0.00	DCE-4	0.73
MCE-3	0.29	DCE-5	0.00
MCE-4	0.00	DCE-6	0.00
MCE-5	0.00	DCE-7	0.69
MCE-6	0.00	DCE-8	0.00
MCE-7	0.02	DCE-9	1.68
MCE-8	0.00	DCE-10	0.00
MCE-9	0.32	DCE-11	0.30
MCE-10	0.00	DCE-12	0.00
MCE-11	0.09	TCE-1	0.00
MCE-12	0.00	TCE-2	0.00
MCE-13	0.00	TCE-3	0.26
MCE-14	0.00	TCE-4	0.12
MCE-15	0.11	TCE-5	0.00
MCE-16	0.00	TCE-6	0.00
MCE-17	0.00	TCE-7	0.10
MCE-18	0.00	TCE-8	0.00
MCE-19	0.00	TCE-9	0.28
MCE-20	0.00	TCE-10	0.24
MCE-21	0.04	TCE-11	0.00
MCE-22	0.00	TCE-12	0.18
MCE-23	0.00	TCE-13	0.00
MCE-24	0.00	TCE-14	0.00
MCE-25	0.00	TCE-15	0.20
MCE-26	0.00	TCE-16	0.00
MCE-27	0.00	TCE-17	0.00
MCE-28	0.00	TCE-18	0.58
DCE-1	0.00	TCE-19	0.38
DCE-2	0.01	TCE-20	0.59

^d CE lists the complex ID that matched with quantified results from experimental data [16], W.F. is the weight factor associated with each CE.

Table 6. The percentage contribution of each structure to the quantified experimental data according to the weighted factor the selected complexes.^e

CE	I22C		D32C		WT(C42)	D52C
	% α 1	% α 3	% α 1	% α 3	% α 3	% α 3
MCE-3	0.00	0.00	0.00	0.00	0.00	16.05
MCE-7	0.00	2.58	0.00	1.05	0.00	0.00
MCE-9	0.00	0.00	0.00	0.00	0.00	16.96
MCE-11	0.00	4.78	0.00	5.07	0.00	0.00
MCE-15	0.00	0.00	0.00	0.00	0.00	7.50
MCE-21	0.00	5.89	0.00	3.18	0.00	0.00
MCE-25	0.00	0.20	0.00	0.08	0.00	0.00
DCE-2	0.00	0.95	0.00	0.43	0.00	0.00
DCE-4	0.00	0.00	0.00	22.62	0.00	0.00
DCE-7	0.00	0.00	0.00	0.00	0.00	16.49
DCE-9	0.00	0.00	67.22	0.00	0.00	0.00
DCE-11	0.00	0.00	0.00	6.14	0.00	12.01
TCE-3	21.03	22.13	0.00	0.00	0.00	0.00
TCE-4	0.00	0.00	0.00	3.82	17.61	5.27
TCE-5	0.00	0.00	0.00	0.00	0.00	0.00
TCE-7	10.88	7.25	2.04	1.93	0.00	0.00
TCE-9	0.00	0.00	0.00	0.00	25.31	13.26
TCE-10	23.90	10.06	0.00	8.24	0.00	0.00
TCE-12	44.20	13.57	8.10	6.03	0.00	0.00
TCE-15	0.00	0.00	0.00	0.00	0.00	12.43
TCE-18	0.00	0.00	0.00	20.14	57.07	0.00
TCE-19	0.00	32.58	0.00	0.00	0.00	0.00
TCE-20	0.00	0.00	22.64	21.20	0.00	0.00

^e % α 1 and % α 3 are the percentage accessibility contribution after the weight factors were associated.

3.2. DC-1 as the Best Predicted Structure

Candidate models were also selected based on Boltzmann population distribution. These models were not subjected to experimental data. In this analysis the binding energy of the candidate models were used in Equation 3 to get the population distribution of the complex of monomer GAPDH with S100A8A9, dimer GAPDH with S100A8A9 and tetramer GAPDH with S100A8A9 separately. The population distribution of the complex of monomer GAPDH with S100A8A9 is presented in Table 7. The probability of MC-1 ($p(\text{MC-1})$) is 0.69, with a binding energy of -63.08 kcal/mol. MC-2 have the second best binding energy of -61.37 kcal/mol, however the $p(\text{MC-2})$ is 0.20 and is quite

Table 7. Monomer Complex categorized and selected based on Boltzmann population distribution.^f

MC	PD	BE	$p(\text{MC})$
MC-1	266	-63.08	0.69
MC-2	1328	-61.37	0.20
MC-3	1715	-60.31	0.09
MC-4	7612	-57.25	0.01
MC-5	3030	-56.87	0.01
MC-6	4262	-56.62	0.01
MC-7	4125	-54.88	0.00
MC-8	13163	-49.83	0.00
MC-9	12564	-48.45	0.00
MC-10	8272	-31.15	0.00
MC-11	9569	-9.85	0.00
MC-12	2930	-1.52	0.00

^f MC represents the complex ID for the monomer GAPDH bound to S100A8A9 that were selected based on their best binding energy. PD is the PatchDock ID number with which the structures can be retrieved from PatchDock web server [28, 29], BE is the binding energy in kcal/mol and $p(\text{MC})$ is the probability associated with each MC from the Boltzmann population distribution.

low compared to MC-1. Similarly MC-3 even though having the third best binding energy, -60.31 kcal/mol, had a $p(\text{MC-3})$ of 0.09. Structures after MC-3 were all ignored for further analysis due to low $p(\text{MC})$. The candidate models selected for the complex of dimer GAPDH with S100A8A9 are presented in Table 8. It is seen that according to the probability analysis DC-1, -76.04 kcal/mol, and DC-2, -76.03 kcal/mol have a difference in binding energy of 0.01 kcal/mol and the $p(\text{DC-1})$ and $p(\text{DC-2})$ for both is 0.38. DC-3 have a binding energy of -75.39 kcal/mol and a $p(\text{DC-3})$ of 0.24. Structures after DC-3 had a $p(\text{DC})$ of 0, therefore these structures were ignored for further analysis as shown in Table 8. Similarly, TC-1 and TC-2 were the only ones chosen for further analysis having a probability of 0.38 and 0.12 respectively as shown in Table 9. The selected candidate

Table 8. Dimer Complex categorized and selected based on the Boltzmann population distribution.^g

DC	PD	BE	$p(\text{DC})$
DC-1	997	-76.04	0.38
DC-2	5	-76.03	0.38
DC-3	1273	-75.39	0.24
DC-4	12482	-48.17	0.00
DC-5	17963	-43.95	0.00
DC-6	18565	-41.09	0.00
DC-7	8431	-39.82	0.00
DC-8	2128	-39.03	0.00
DC-9	15223	-18.443	0.00
DC-10	4237	-14.95	0.00
DC-11	11000	-11.49	0.00
DC-12	4848	-0.45	0.00

^gDC represents the ID for the dimer GAPDH bound to S100A8A9, that were selected based on their best binding energy, PD is the PatchDock ID number with which the structures can be retrieved from PatchDock web server [28, 29], BE is the binding energy in kcal/mol and $p(\text{DC})$ is the probability associated with each DC from the Boltzmann population distribution.

models based on Boltzmann population distribution and the models based on partial experimental match are summarized in Figure 2. There was a total of 6 structures, as shown in Figure 2A found where the monomer GAPDH bound to S100A8A9 showed

Table 9. Tetramer Complex categorized and selected based on the Boltzmann population distribution.^h

TC	PD	BE	<i>p</i>(TC)
TC-1	4098	-43.44	0.88
TC-2	13548	-40.67	0.12
TC-3	20509	-34.66	0.00
TC-4	12232	-33.79	0.00
TC-5	16505	-33.22	0.00
TC-6	7429	-31.48	0.00
TC-7	14804	-27.16	0.00
TC-8	14623	-25.39	0.00
TC-9	1879	-19.98	0.00
TC-10	22300	-1.45	0.00

^hTC represents the ID for the tetramer GAPDH bound to S100A8A9, that were selected based on their best binding energy, PD is the PatchDock ID number with which the structures can be retrieved from PatchDock web server [28, 29], BE is the binding energy in kcal/mol and *p*(DC) is the probability associated with each DC from the Boltzmann population distribution.

partial match to experimental data had weight factor associated with them. A total of 4 structures for the dimer GAPDH bound to S100A8A9 were found with their significant weight factor that corresponds to their partial match to the overall quantified experimental data as shown in Figure 2B. A total of 10 structures for the tetramer GAPDH bound to S100A8A9 were found with their corresponding weight factor are shown in Figure 2C. From the Boltzmann population distribution a total of 8 structures were found, where 3 structures were for the monomer GAPDH, 2 structures for the tetramer GAPDH and 3 structures for the dimer GAPDH were found that were bound to S100A8A9 as shown in Figure 2D, 2E and 2F.

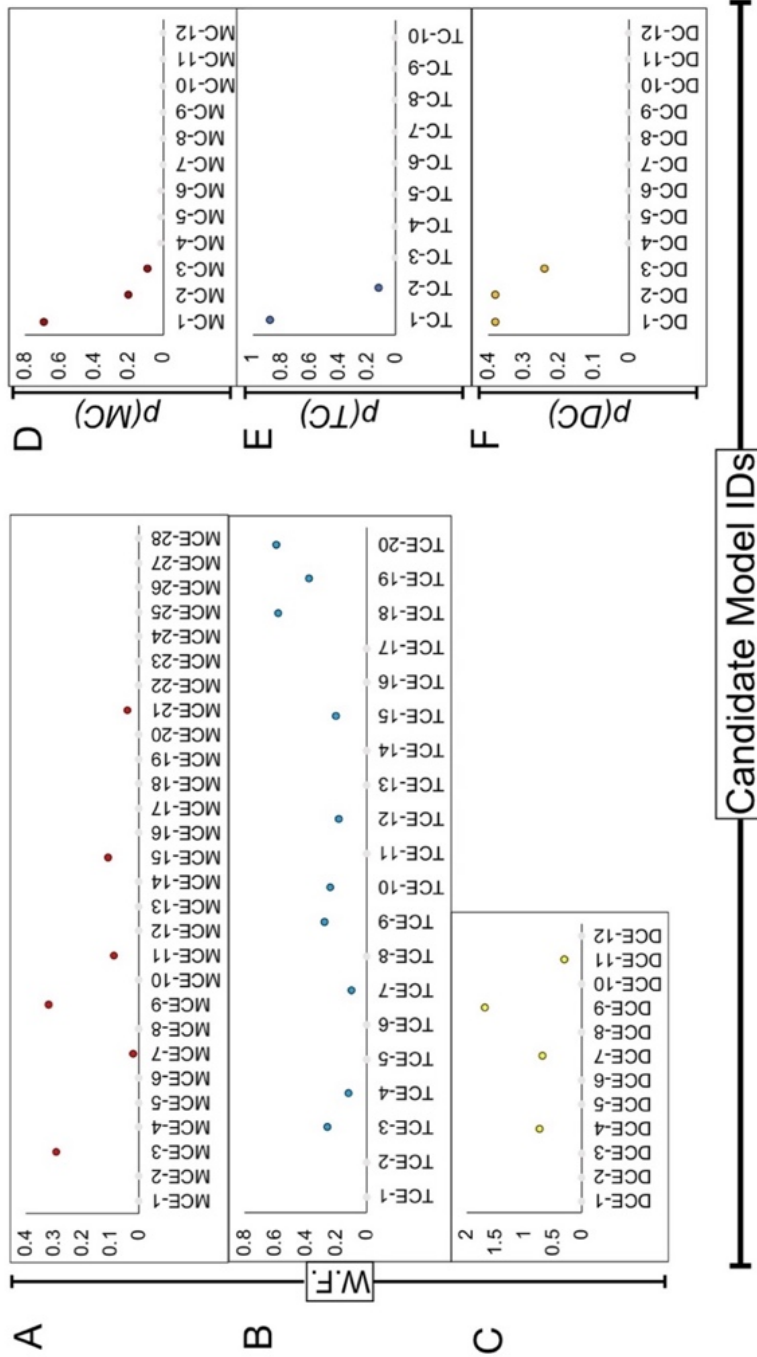


Figure 2. W.F. is the weight factor associated for all complexes in (A), (B) and (C). p(MC), p(DC) and p(TC) are probabilities of all complexes in (D), (E) and (F). All grey circular dots were omitted due to low W.F. Red (A), blue (B), yellow (C), Darker red (D), darker blue (E), darker yellow (F) circular dots represents the MCEs, TCEs, DCEs, MCs, TCs and the DCs that were selected for further analysis

3.3. Interaction Energies of Predicted Complexes

The interface residues for MCE-9 are shown in Figure 3A. When a single point

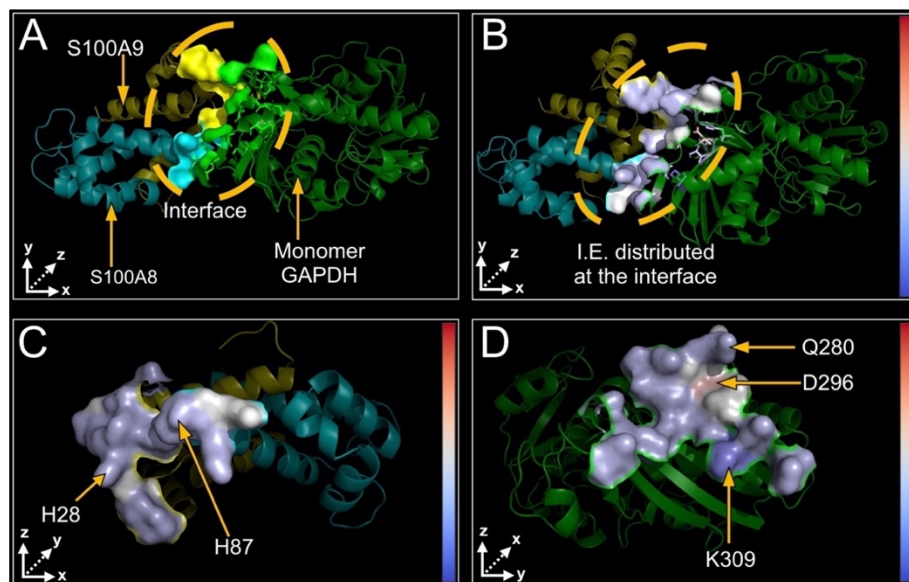


Figure 3. (A) MCE9 consists of S100A9 (yellow), S100A8 (cyan) and monomer GAPDH. (B) Interaction energies (I.E.) of residues distributed at the interface of the binding subunits. (C) H87 on S100A8 and H28 on S100A9 have high attractive interaction with GAPDH. (D) K309 and Q280 have high attractive interactions with S100A8A9 and D296 have high repulsive interactions with S100A8A9.

energy calculations was done on the minimized structure of MCE-9 to obtain the interaction energy distribution, as shown in Figure 3B, it was seen that H28 on S100A8 had the largest attractive interaction, -46.74 kcal/mol as presented in Table 10 and shown in Figure 3C. The shortest distance of H28 to its opposing binding subunit, GAPDH is 2.87Å. The interface residue on GAPDH that had the strongest attractive interaction energy, -102.40 kcal/mol, with S100A8A9 was K309 with a shortest distance of 2.87Å, presented in Table 10 and Figure 3D. There is also a presence of a moderately strong

Table 10. The following interface residues, in MCE-9 and MC-1, were shown to have the most to the interaction energies with their binding partners ⁱ

MCE-9					
S100A8A9	I.E.	Distance (1)	GAPDH	I.E.	Distance (2)
H87A	-46.74	2.87	Q280O	-27.87	2.39
H28C	-24.72	3.58	D296O	79.75	3.31
			K309O	-102.40	2.87
MC-1					
D59A	-87.00	3.10	R13O	-126.88	2.09
D63A	-99.96	2.84	R16O	-122.00	3.11
E70A	-76.36	2.98	K186O	-119.55	4.20
			R200O	-97.68	4.72
			E317O	79.59	3.29

ⁱS100A8A9 represents the interface residues of chains A and C. S100A8 and S100A9 are represented by chain A and C respectively. Therefore the naming convention of this column is : One letter code of the amino acid, followed by the position of the amino acid, followed by the chain of the protein. GAPDH represents the interface residues of the monomer GAPDH and the column follows similar naming convention to S100A8A9. Distance are represented in Å and it is the shortest distance between two residues at the interface within 5Å. Distance (1) is the shortest distance calculated from each S100A8A9 residue to GAPDH. Distance (2) is the shortest distance calculated from each GAPDH residues to S100A8A9. I.E. represents the short-range interaction energy between a residue and its opposing binding subunit in kcal/mol.

repulsive interaction of 79.75 kcal/mol from GAPDH interface residue D296 as indicated Figure 3D. On the other hand, MC-1 had more interface residues with strong attractive interactions as shown in Table 10 and Figure 4. Figure 4A and 4B are the interface residues and the distribution of the interaction energies for MC-1 after a single point energy calculation. The strongest attractive interaction energy, -99.96 kcal/mol coming from the residue of S100A8A9 interface was D63 on the protein S100A8 and the shortest distance calculated to its opposing binding subunit was 2.84Å as indicated in Figure 4C. The strongest attractive interaction from the GAPDH interface was coming

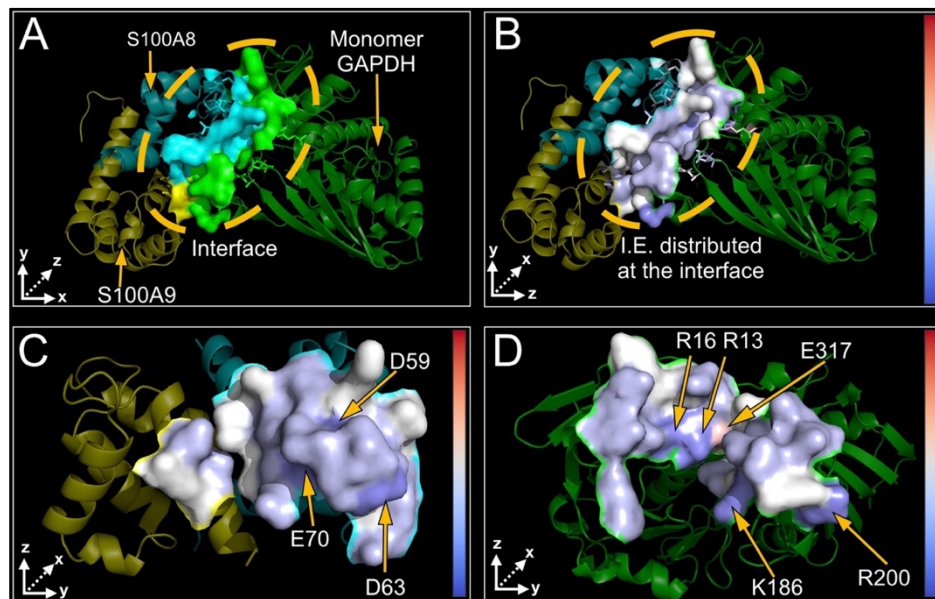


Figure 4. (A) MC1 consists of S100A9 (yellow), S100A8 (cyan) and monomer GAPDH. (B) Interaction energies (I.E.) of residues distributed at the interface of the binding subunits. (C) D59, D63 and E70 on S100A8 have the high attractive interactions with GAPDH. (D) R13, R16, K186 and R200 on GAPDH have high attractive interactions with S100A8A9.

from residue R13, -126.88 kcal/mol, and the shortest distance calculated was 2.09Å. A moderate repulsion, 79.59 kcal/mol, is also felt by S100A8A9 binding subunit in MC-1 from E317 of GAPDH as shown in Figure 4D. In DCE-9 as shown in Figure 5A, it is seen that the binding of S100A8A9 to GAPDH is stronger on one of the two chains as shown in Figure 5B. D14 on the protein S100A8, Figure 5C, has the highest interaction of energy of -92.50 kcal/mol and K219 has the highest attractive interaction energy, -106.61 kcal/mol, on the dimer GAPDH. The shortest distance that was found for D14 to GAPDH is 4.61Å and the shortest distance for K219 is 2.61Å. There is also a high repulsion from D127 of GAPDH at the interface as shown in Figure 5D. In DC-1 as

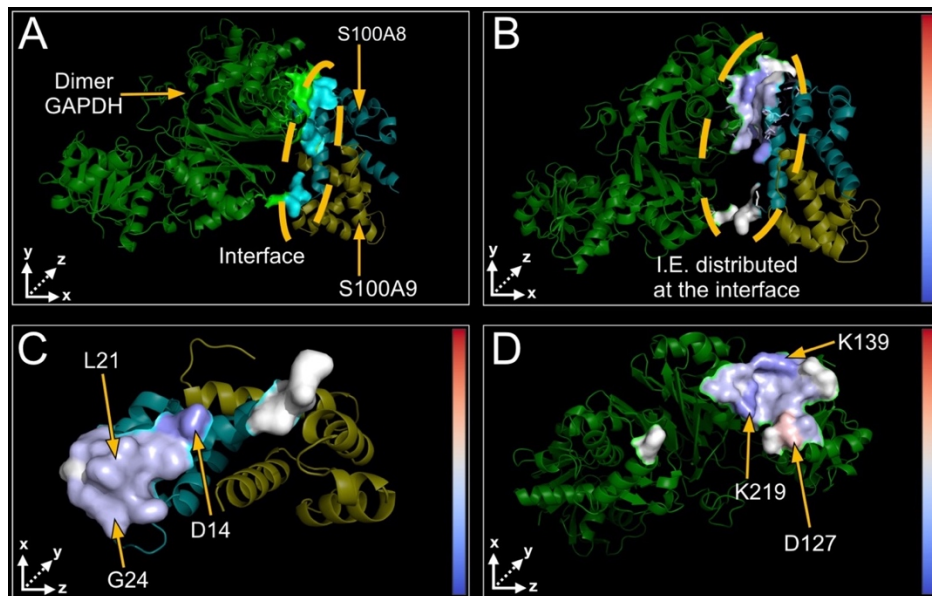


Figure 5. (A) DCE9 consists of S100A9 (yellow), S100A8 (cyan) and dimer GAPDH. (B) Interaction energies (I.E.) of residues distributed at the interface of the binding subunits. (C) D14, L21 and G24 have high attractive interactions with dimer GAPDH. (D) K139 and K219 have high attractive interactions and D127 have high repulsive interactions with S100A8A9.

shown in Figure 6A and its distribution of the interaction energy shown in Figure 6B of the interface residues show that D63 on S100A8, Figure 6C, and K55 on the dimer GAPDH, Figure 6D, have the highest attractive energy and are both below a distance of 3Å. In DC-1, the interaction energy is well distributed in both the chains of the dimer GAPDH. Even though there are two repulsive interactions from D285 and D289, attractive interactions dominate the dimer GAPDH interface within the binding site. From Table 11, it is also seen that E317 that was present in MC-1 as a repulsive interaction is also present in DC-1. In TCE-20, D14 on S100A8A9 had the strongest attractive interaction, -139.94 kcal/mol, with GAPDH and the shortest distance was 2.23Å. On the interface of GAPDH it was E250 with an attractive interaction energy of

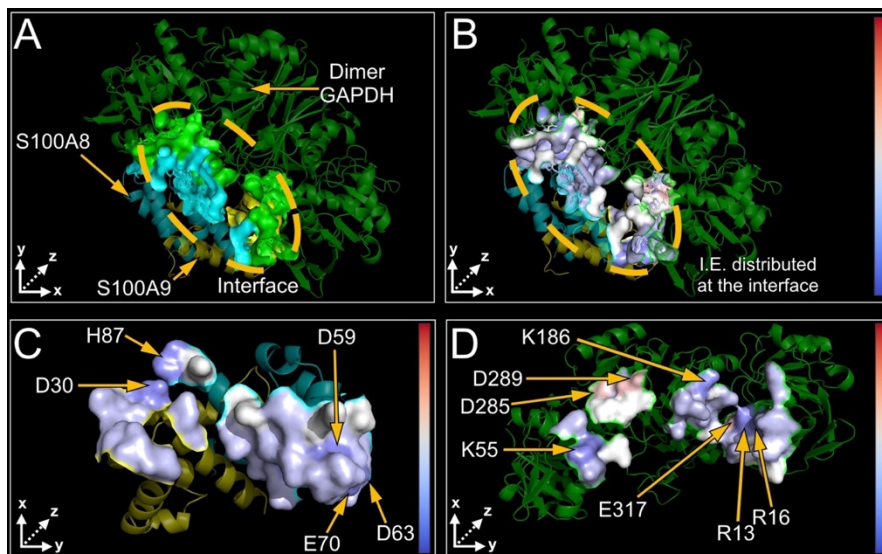


Figure 6. (A) DC1 consists of S100A9 (yellow), S100A8 (cyan) and dimer GAPDH (green). (B) Interaction energies (I.E.) of residues distributed at the interface of the binding subunits. (C) D30 of S100A9 and D59, D63, E70 and H87 of S100A8 have high attractive interactions with dimer GAPDH. (D) R13, R16, K55 and K186 on dimer GAPDH have attractive interactions and D285, D289 and E317 have interactions with S100A8A9.

Table 11. The following interface residues, in DCE-9 and DC-1, were shown to have the most to the interaction energies with their binding partners^j

DCE-9					
S100A8A9	I.E.	Distance (1)	GAPDH	I.E.	Distance (2)
D14A	-92.50	4.61	D127O	93.91	2.29
L21A	-21.46	4.66	K139O	-97.54	2.44
G24A	-21.85	2.44	K219O	-106.61	2.61
F26A	-10.37	2.72			
DC-1					
D59A	-111.67	3.08	K55O	-138.04	2.52
D63A	-120.10	2.94	D285O	115.20	2.79
H87A	-100.25	2.27	D289O	107.56	4.94
E70A	-91.84	3.06	R13P	-122.68	2.89
D30C	-94.51	4.59	R16P	-121.15	3.35
			K186P	-129.02	3.34
			E317P	77.51	3.50

^j See footnote of Table 10 for the explanations

-134.49 kcal/mol and the shortest distance to S100A8A9 was 2.08Å. In TC-1 the attractive interactions for D14A was much stronger, -185.39 kcal/mol, but so were the repulsive interactions coming from K18 and K23 of S100A8A9 of the binding subunit. The attractive interaction energy of TC-1 is much lower than it was seen on TCE-20 with the strongest interaction coming from K55, -78.48 kcal/mol as shown in Table 12. In both

Table 12. The following interface residues, in TCE-20 and TC-1, were shown to have the most to the interaction energies with their binding partners ^k

TCE20					
S100A8A9	I.E.	Distance (1)	GAPDH	I.E.	Distance (2)
D14A	-139.94	2.23	E250O	-134.9	2.08
K18A	88.88	4.89	K219P	-109.72	2.80
K23A	72.58	4.60	K227P	-88.48	2.49
K54C	-25.24	2.68	E250P	-51.16	2.17
TC-1					
D14A	-185.39	2.89	R20P	-61.98	4.31
K18A	101.33	2.08	K61P	-44.58	4.37
K23A	137.49	4.16	K55R	-78.48	3.11
D63A	-154.12	2.42			
K51C	88.48	4.09			

^k See footnote of Table 10 for explanations

TCE-20 and TC-1, the S100A8A9 bound to the tetramer GAPDH on two out of the four chains of GAPDH. The interface residues of S100A8A9 with strong interactions in TCE-20 were also present in TC-1. In both cases, there were more repulsions seen in tetramer GAPDH bound to S100A8A9, as shown in Figure 7 and 8, when compared to MCE-9, MC-1, DCE9 and DC-1. This suggests a general trend of increasing repulsion among the residues were seen as the size of the GAPDH increased from a monomer to a tetramer across the best 6 candidate models. The interaction energies for all interface residues among all chosen candidate models are presented in Figure 9, 10, 11, 12, 13 and 14.

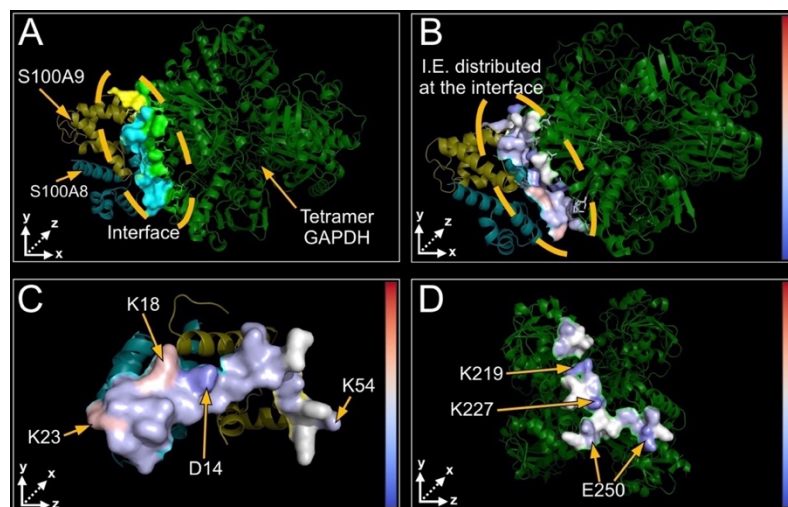


Figure 7. (A) TCE20 consists of S100A9 (yellow), S100A8 (cyan) and tetramer GAPDH (green). (B) Interaction energies (I.E.) of residues distributed at the interface of the binding subunits. (C) D14 of S100A8 and K54 of S100A9 have high attractive interactions and K18 and K23 have high repulsive interactions with tetramer GAPDH. (D) K219 and K227 on tetramer GAPDH have attractive interactions with S100A8/A9.

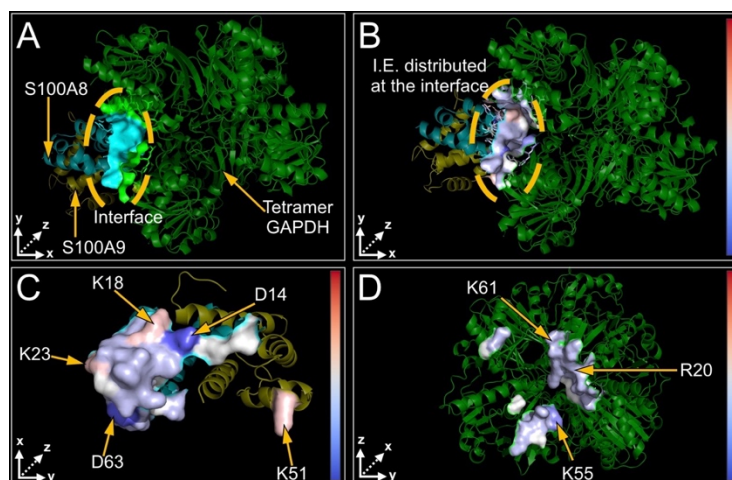


Figure 8. (A) TC1 consists of S100A9 (yellow), S100A8 (cyan) and tetramer GAPDH (green). (B) Interaction energies (I.E.) of residues distributed at the interface of the binding subunits. (C) D14 and D63 of S100A8 have high attractive interactions and K18, K23 and K51 have high repulsive interactions with tetramer GAPDH. (D) R20, K55 and K61 on tetramer GAPDH have attractive interactions with S100A8/A9.

Among these figures the residues with strong interaction energies are highlighted and are presented in details in Appendix A.

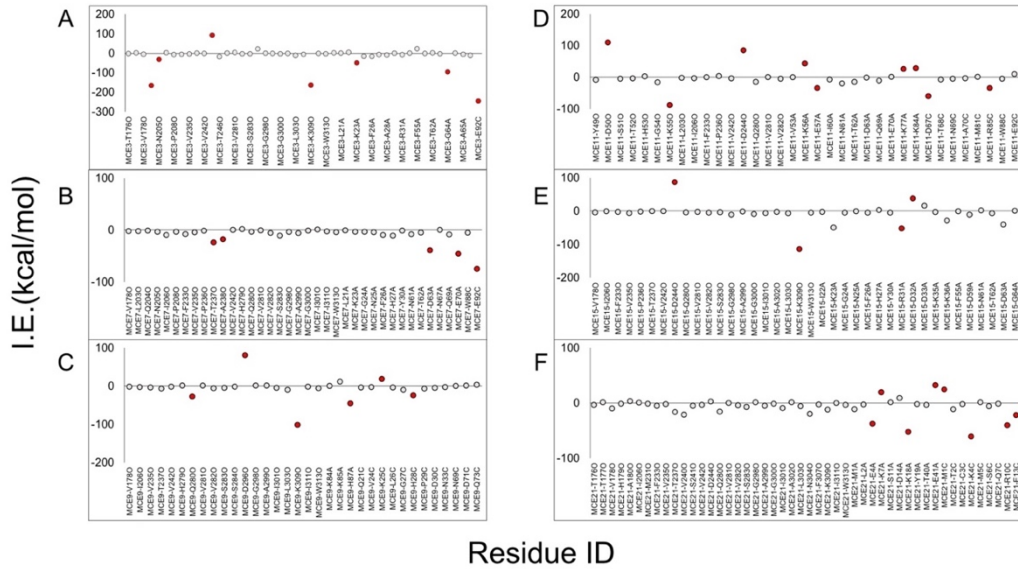


Figure 9. Interaction energies of interface residues of the binding subunits (GAPDH and S100A8A9) of MCE-3 (A), MCE-7(B), MCE-9 (C), MCE-11 (D), MCE-15 (E) and MCE-21 (F). Strong interactions of MCEs are indicated in red circular dots.

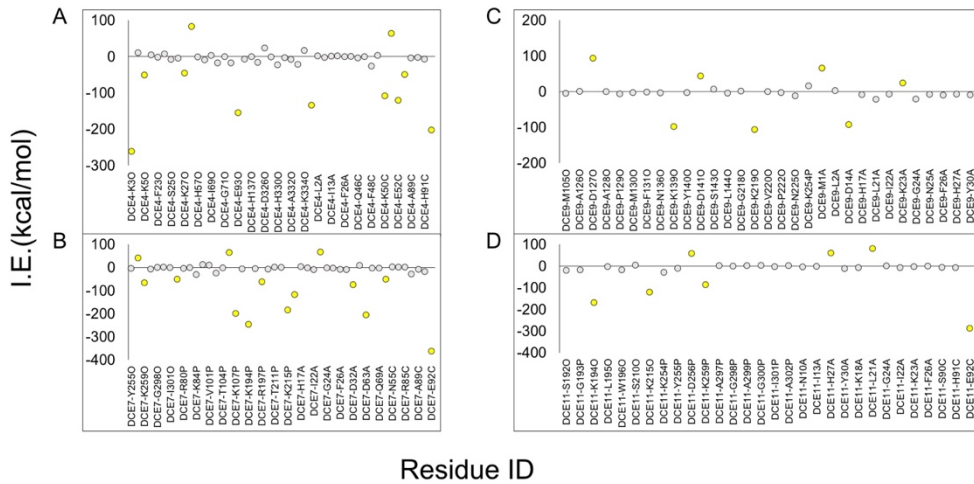


Figure 10. Interaction energies of interface residues of the binding subunits (GAPDH and S100A8A9) of DCE-4 (A), DCE-7 (B), DCE-9 (C) and DCE-11 (D). Strong interactions of DCEs are indicated in yellow circular dots.

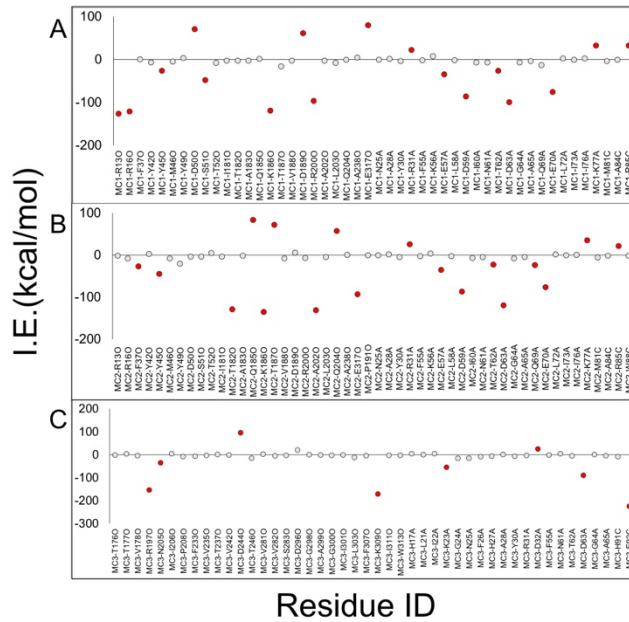


Figure 13. Interaction energies of interface residues of the binding subunits (GAPDH and S100A8A9) of MC-1 (A), MC-2 (B) and MC-3 (C). Strong interactions of MCs are indicated in red circular dots.

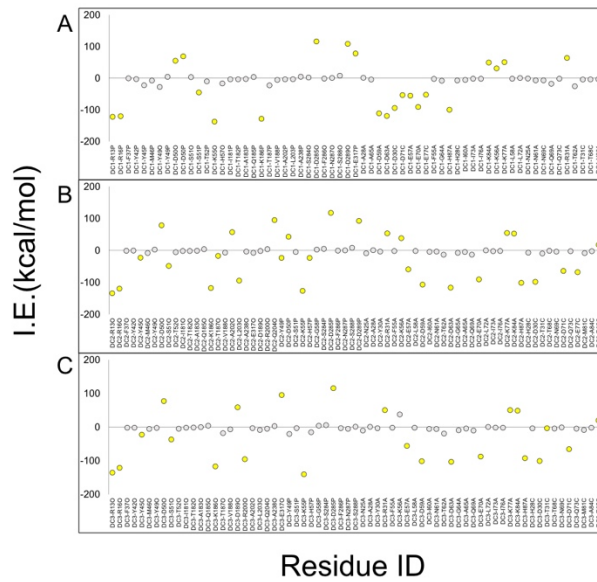


Figure 14. Interaction energies of interface residues of the binding subunits (GAPDH and S100A8A9) of DC-1 (A), DC-2 (B) and DC-3 (C). Strong interactions of DCs are indicated in yellow circular dots.

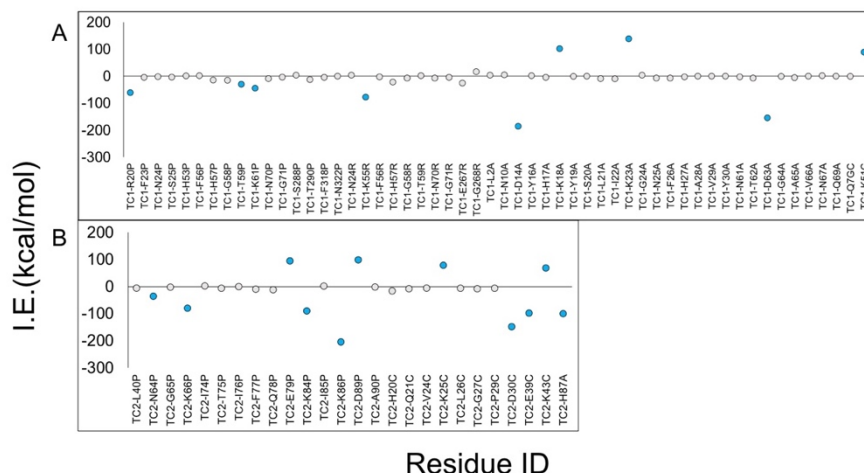


Figure 15. Interaction energies of interface residues of the binding subunits (GAPDH and S100A8A9) of TC-1 (A) and TC-2 (B). Strong interactions of TCs are indicated in blue circular dots.

3.4. Alanine Scanning Results suggest Destabilization with Size

Virtual alanine scanning results of the complex of MCE-9 and MC-1 showed that MCE-9 has less interface residues contributing to the destabilization of the complex than MC-1 as shown in Figure 16. Similar results were also obtained when DCE-9 was MCE-9 the most as shown in Figure 16A and 16B. Figure 16C and 16D are the alanine scanning results of MC-1, where the interface residues that destabilized the protein complex the most were D59 and I60 on S100A8 of S100A8A9 and R13, D50, T182, Q185, and E317 on GAPDH. Results of MC-1 suggest that this a much better docking compared to MCE-9. In case of DCE-9, F26 on S100A8 of S100A8A9 and F131, N136, Y140 of the dimer GAPDH caused the most destabilization of the complex as shown in Figure 17A and 17B. In DC-1, the residues responsible for destabilization the complex were the same as the residues responsible for the destabilization of MC-1 as presented in Figure 17C and 17D. In TCE-9 the F26 on S100A8 shown in Figure 18A

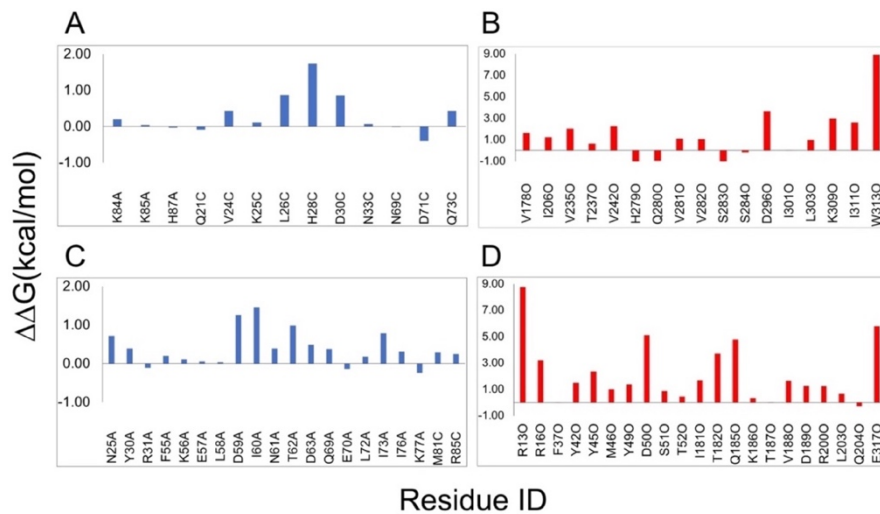


Figure 16. Alanine scanning of S100A8A9 with monomer GAPDH shows that structure that matched with experimental data had less interface residues when compared to structure predicted from Boltzmann population distribution. **(A)** H28 on S100A9 of the binding subunit S100A8A9 resulted in the most destabilization upon mutation to alanine in MCE-9. **(B)** W313 shows the most destabilization on GAPDH in MCE-9. **(C)** D59 and I60 on S100A8 of S100A8A9 showed considerable destabilization of the complex MC-1. **(D)** R13, D50, T182, Q185, and E317 on GAPDH destabilizes MC-1.

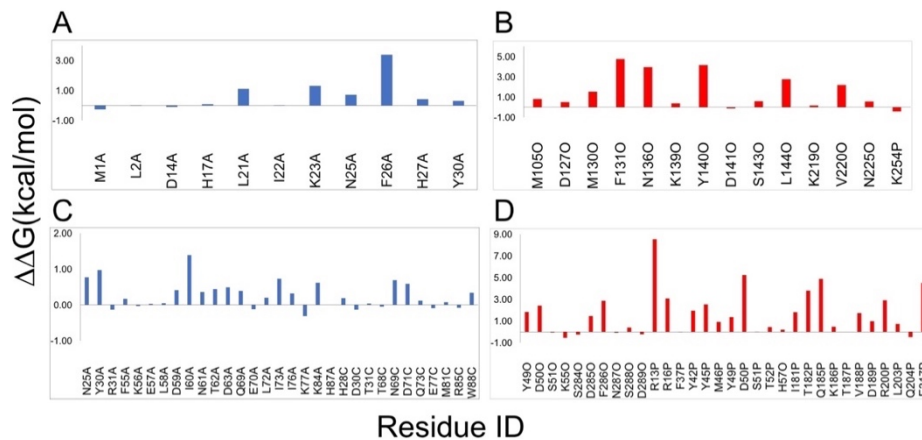


Figure 17. Alanine scanning of S100A8A9 with dimer GAPDH shows that structure that matched with experimental data had less interface residues when compared to structure predicted by Boltzmann population distribution. **(A)** F26 on S100A8 of the binding subunit S100A8A9 resulted in the most destabilization upon mutation to alanine in DCE-9. **(B)** F131, N136 and Y140 shows the most destabilization on GAPDH in DCE-9. **(C)** N25, Y30 and I60 on S100A8 of S100A8A9 showed considerable destabilization of the complex DC-1. **(D)** R13, D50, T182, Q185, and E317 on GAPDH destabilizes have shown considerable destabilization of GAPD in DC-1.

again caused the most destabilization of the complex. F26 is also present in TC-1 along with L21, I22, N25 and T62 on S100A8 as shown in Figure 18C. The residues on the GAPDH interface of TCE-20 causing the most destabilization, Figure 18B, upon mutation were L249, V171, L224, R248 and L249. But in TC-1 these interface residues,

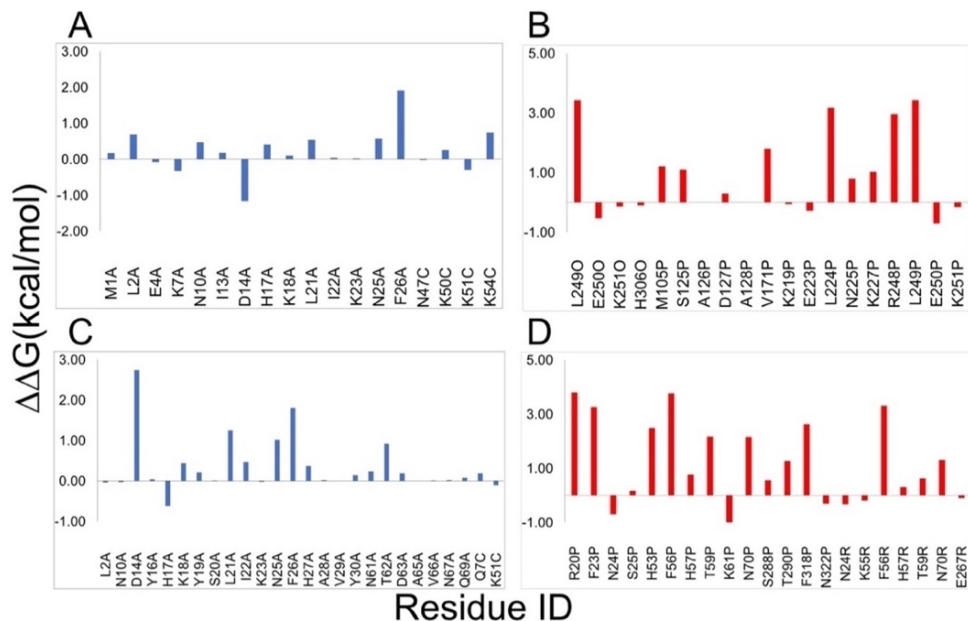


Figure 18. Alanine scanning results of the complex of S100A8A9 with tetramer GAPDH shows that structure that matched with experimental data had less interface residues when mutated alanine destabilized the protein when compared to structure predicted by Boltzmann population distribution. **(A)** F26 on S100A8 of the binding subunit S100A8A9 resulted in the most destabilization upon mutation to alanine in TCE-20. **(B)** L249, V171, L224 R248 and L249 cause the most destabilization on GAPDH in TCE-20. **(C)** D14, L21, I22, N25, F26 and T62 on S100A8 of S100A8A9 showed considerable destabilization of the complex TC-1. **(D)** R20, F23, H53, F56 (chain P), T59, F318 and F56(chain R) have shown to destabilize the complex TC-1

Figure 18D, were not common among other candidate with F56 showing up twice on the tetramer GAPDH. It was also noted that as the size of GAPDH increased from a monomer to tetramer, the interface residues of S100A8A9, responsible for the

destabilization, for the best 6 candidate model shifted more towards S100A8. Complete virtual alanine scanning results for interface residues of all candidate models are presented in Appendix B.

3.5. Analysis of the AINT Method

The virtual screening method is based on the experimental technique of mapping protein-protein interactions by localized oxidation using hydroxyl radical [22], to select candidate models from the PatchDock algorithm. Proteins are highly dynamic in nature however when compared to a hydroxyl radical, proteins generally have diffusion coefficient that is less than 1% [22]. Therefore in calculating AINT and the interaction energies, the protein was also treated as still geometries. Since the literature suggests the average distance, between C α of an engineered residue to an oxidized residue was $22.3 \pm 7.9\text{\AA}$ [22], in our analysis we took a distance of 25\AA . When we applied this analysis to our virtual screening, we found structures that where the GAPDH and S100A8A9 are weakly bound to each other. This is expected, since artificially placing a FeBABE arm on S100A8A9 is likely to cause a conformational shift of the protein and this will in turn change how the protein interact with GAPDH. Therefore our method enabled us to look at protein structures that would typically be ignored by Boltzmann population sampling. However, this method may not be sufficient enough to guide us to the true structure of the protein. It was because of this reason we looked at the best docking provided by the PatchDock algorithm [28, 29], since the algorithm relies on shape complementarity criteria, where one can envision the assembling of these complexes similar to that of trying to match two pieces of a jigsaw puzzle [28], we also analyzed these docking even when they did not match with the experimental data [16].

Furthermore, in our AINT calculation, where FeBABE arm was attached to Cys side chain, the arm has several rotational freedom about several single bond [22], however we based our AINT calculation restricted to a single dimension from where the arm had a clear path to the $\alpha 1$ and $\alpha 3$ [24] helices of GAPDH and was in the range of 25Å, however for a full accessibility all other degrees of freedom must also be explored. Therefore our accessibility calculation as presented in Equation 1 needs further modifications to accommodate several other single bond rotations. There are several applications that can be implemented with this method. This method upon further modification can be implemented as a plugin in docking algorithm as a post refinement method and is in consideration for future works. Since FIREDock [29, 30] uses CHARMM19 force field [47] to do binding energy prediction , these binding energies may also be over estimates of the true binding energy of the complexes presented and there has been significant improvement in CHARMM force field [43, 44] since the of release CHARMM19 force field. Therefore is still a need to accurately predicting the binding energy of these selected complexes to further filter out models that are unlikely to form. A QMMM study to observe how the hydroxyl radical is being transported to the target protein and benchmarking across a large number of other experimental protein-protein interaction dataset is also required to statistically validate this method.

CHAPTER IV

CONCLUSION

In this theoretical work, a simple virtual artificial protease method is presented to sample protein-protein docking of GAPDH and S100A8A9. These docking's interface residues were further analyzed with virtual alanine scanning with Robetta Web Server [33] and their interaction energies are calculated using GROMACS 2016 [34, 35, 36, 37, 38, 39, 40, 41]. Analysis from both the interaction energies and virtual alanine scanning points to similar interface residues among the best candidates when sampled using Boltzmann population distribution. The virtual artificial protease method however leads to different structures that matches with experimental data as an ensemble. We have also analyzed the interface residues of potential structures by virtual alanine scanning and interaction energy calculations in hopes to aide experimentalists with a potential lead to mutate a residue within this complex of GAPDH and S100A8A9.

REFERENCES

1. Gebauer, F.; Hentze, MW. Molecular mechanisms of translational control. *Nat. Rev. Mol. Cell Biol.* **2004**, 5, 827–835.
2. Wilkie, GS.; Dickson, KS.; Gray, NK. Regulation of mRNA translation by 5'- and 3'-UTR-binding factors. *Trends Biochem. Sci.* **2003**, 28, 182–188.
3. Mazumder, B.; Seshadri, V.; Fox, PL. Translational control by the 3'-UTR: the ends specify the means. *Trends Biochem. Sci.* **2003**, 28, 91–98.
4. Mukhopadhyay, R.; Jia, J.; Arif, A.; Ray, PS.; Fox, PL. The GAIT system: a gatekeeper of inflammatory gene expression. *Trends Biochem. Sci.* **2009**, 34, 324–331.
5. Vyas, K; et al. Genome-wide polysome profiling reveals an inflammation-responsive posttranscriptional operon in gamma interferon-activated monocytes. *Mol. Cell. Biol.* **2009**, 29, 458–470.
6. Sampath, P.; et al. Noncanonical function of glutamyl-prolyl-tRNA synthetase: gene-specific silencing of translation. *Cell.* **2004**, 119, 195–208.
7. Ferrara, N.; Davis-Smyth, T. The biology of vascular endothelial growth factor. *Endocr Rev.* **1997**, 18, 4–25.
8. Coussens, LM.; Werb, Z. Inflammation and cancer. *Nature.* **2002**, 420, 860–867.
9. Seth, D.; Hausladen, A.; Wang, Y-J.; Stamler, JS. Endogenous protein S-nitrosylation in *E. coli*: regulation by OxyR. *Science (New York, NY).* **2012**, 336, 6080.
10. Seth, D.; Stamler, JS. The SNO-proteome: Causation and Classifications. *Current opinion in chemical biology.* **2011**, 15 (1), 129-136.

11. Haldar, SM.; Stamler, JS. S-nitrosylation: integrator of cardiovascular performance and oxygen delivery. *J. Clin. Investig.* **2013**, 123 (1), 101-110.
12. Lim, K-H.; Ancrile, BB.; Kashatus. DF.; Counter, CM. Tumour maintenance is mediated by eNOS. *Nature.* **2008**, 452 (7187), 646-649.
13. Nakamura, T.; Lipton, SA.; Emerging Role of Protein-Protein Transnitrosylation in Cell Signaling Pathways. *Antioxid. Redox Signal.* **2013**, 18 (3), 239-249.
14. Jia, J.; Arif, A.; Terenzi, F.; et al. Target-selective Protein S-Nitrosylation by Sequence Motif Recognition. *Cell.* **2014**, 159 (3), 623-634.
15. Padgett. C.M.; Whorton, A.R. S-nitrosoglutathione reversibly inhibits GAPDH by S-nitrosylation. *Am. J. Physiol.* **1995**, 269 (3), 739-749.
16. Jia. J.; Arif. A.; Stuehr. DJ.; Hazen. SL.; Fox, PL. Protection of Extraribosomal RPL13a by GAPDH and Dysregulation by S-Nitrosylation. *Mol. Cell.* **2012**, 47(4), 656-663.
17. Croce, K.; Gao, H.; Wang. Y.; et al. MRP-8/14 is Critical for the Biological Response to Vascular Injury. *Circulation.* **2009**, 120 (5), 427-436.
18. Ionita, M.G.; Vink, A.; Dijke, I.E.; Laman, J.D.; Peeters, W.; van der Kraak, P.H.; Moll, F.L.; de Vries, J.P.; Pasterkamp, G.; de Kleijn, D.P. High levels of myeloid-related protein 14 in human atherosclerotic plaques correlate with the characteristics of rupture-prone lesions. *Arter. Thromb. Vasc. Biol.* **2009**, 29, 1220–1227.
19. McCormick, M.M.; Rahimi, F.; Bobryshev, Y.V.; Gaus, K.; Zreiqat, H.; Cai, H.; Lord, R.S.; Geczy, C.L. S100A8 and S100A9 in human arterial wall. Implications for atherogenesis. *J. Biol. Chem.* **2005**, 280, 41521-41429.

20. Ha, T-Y.; Chang, K-A.; Kim, J a.; et al. S100a9 Knockdown Decreases the Memory Impairment and the Neuropathology in Tg2576 Mice, AD Animal Model. Amédée T, ed. *PLoS ONE*. 2010, 5 (1), e8840.
21. Nathan, C.; Calingasan, N.; Nezezon, J. et al. Protection from Alzheimer's-like disease in the mouse by genetic ablation of inducible nitric oxide synthase. *J. Exp. Med.* **2005**, 202 (9), 1163-1169.
22. Cheal, SM.; Ng, M.; Barrios, B.; Miao, Z.; Kalani, AK.; Meares, CF. Mapping Protein-Protein Interactions by Localized Oxidation: Consequences of the Reach of Hydroxyl Radical. *Biochemistry*. **2009**, 48 (21), 4577-4586.
23. Korndörfer, IP1.; Brueckner, F.; Skerra, A. The crystal structure of the human (S100A8/S100A9)₂ heterotetramer, calprotectin, illustrates how conformational changes of interacting alpha-helices can determine specific association of two EF-hand proteins. *J Mol Biol.* **2007**, 370 (5), 887-98.
24. Ismail, SA.; Park, HW. Structural analysis of human liver glyceraldehyde-3-phosphate dehydrogenase. *Acta Crystallogr., Sect. D: Biol. Crystallogr.* **2005**, 61 (11), 1508-13.
25. Engel, M.; Seifert, M.; Theisinger, B.; Seyfert, U.; Welter, C. Glyceraldehyde-3-phosphate dehydrogenase and Nm23-H1/nucleoside diphosphate kinase A. Two old enzymes combine for the novel Nm23 protein phosphotransferase function. *J Biol Chem.* **1998**, 273 (32), 58-65.
26. Carlile, GW.; Chalmers-Redman, RM.; Tatton, NA.; Pong, A.; Borden, KE.; Tatton, WG. Reduced apoptosis after nerve growth factor and serum withdrawal: conversion

- of tetrameric glyceraldehyde-3-phosphate dehydrogenase to a dimer. *Mol Pharmacol.* **2000**, 57 (1), 2-12.
27. Duhovny, D.; Nussinov, R.; Wolfson, HJ. Efficient Unbound Docking of Rigid Molecules. In Gusfield et al., Ed. Proceedings of the 2'nd Workshop on Algorithms in Bioinformatics(WABI) Rome, Italy, Lecture Notes in Computer Science. *Springer.* **2002**, 2452, 185-200.
28. Schneidman-Duhovny, D.; Inbar, Y.; Nussinov, R.; Wolfson, HJ. PatchDock and SymmDock: servers for rigid and symmetric docking. *Nucl. Acids. Res.* **2005**, 33, 363-367.
29. Andrusier, N.; Nussinov, R.; Wolfson, HJ. FireDock: Fast Interaction Refinement in Molecular Docking. *Proteins*, **2007**, 69 (1), 139-59.
30. Mashiach, E.; Schneidman-Duhovny, D.; Andrusier, N.; Nussinov, R.; Wolfson, HJ. FireDock: a web server for fast interaction refinement in molecular docking. *Nucleic Acids Res.* **2008**, 36 (Web Server issue), W229-W232.
31. Schneider, CA.; Rasband, WS.; Eliceiri, KW. "NIH Image to ImageJ: 25 years of image analysis", *Nature methods.* **2012**. 9(7), 671-675
32. Firoz, A.; Malik, A.; Afzal, O.; Jha, V. ContPro: A web tool for calculating amino acid contact distances in protein from 3D -structure at different distance threshold. *Bioinformatics.* **2010**, 5 (2), 55-57.
33. Kim DE, Chivian D, Baker D. Protein structure prediction and analysis using the Robetta server. *Nucleic Acids Res.* **2004**, 32 (Web Server issue), W526-W531

34. Bekker, H.; Berendsen, HJC.; Dijkstra, EJ.; Achterop, S.; van Drunen, R.; van der Spoel, D.; Sijbers, A.; Keegstra, H.; Reitsma, B.; Renardus, MKR. Gromacs: A parallel computer for molecular dynamics simulations. *World Scientific*. **1993**, 92.
35. Berendsen, HJC.; van der Spoel, D.; van Drunen, R. GROMACS: A message-passing parallel molecular dynamics implementation. *Comp. Phys. Comm.* **1995**, 91, 43–56.
36. Lindahl, E.; Hess, B.; van der Spoel, D. GROMACS 3.0: A package for molecular simulation and trajectory analysis. *J. Mol. Mod.* **2001**, 7, 306–317.
37. van der Spoel, D.; Lindahl, E.; Hess, B.; Groenhof, G.; Mark, A. E.; Berendsen, HJC. GROMACS: Fast, Flexible and Free. *J. Comp. Chem.* **2005**, 26, 1701–1718.
38. Hess, B.; Kutzner, C.; van der Spoel, D., Lindahl, E. GROMACS 4: Algorithms for Highly Efficient, Load-Balanced, and Scalable Molecular Simulation. *J. Chem. Theory Comput.* **2008**, 4 (3), 435–447.
39. Pronk, S.; Páll, S.; Schulz, R.; Larsson, P.; Bjelkmar, P.; Apostolov, R.; Shirts, M. R.; Smith, JC.; Kasson, PM.; van der Spoel, D.; Hess, B.; Lindahl, E. GROMACS 4.5: A highthroughput and highly parallel open source molecular simulation toolkit. *Bioinformatics*. **2013**, 29 (7), 845–854.
40. Páll, S.; Abraham, MJ.; Kutzner C.; Hess B.; Lindahl, E. Tackling Exascale Software Challenges in Molecular Dynamics Simulations with GROMACS. In: Markidis, S.; Laure, E. (eds) Solving Software Challenges for Exascale. Lecture Notes in Computer Science. *Springer Cham*. **2015**, 8759.

41. Abraham, MJ.; Murtola, T.; Schulz, R.; Páll, S.; Smith, JC.; Hess, B.; Lindahl, E.
GROMACS: High performance molecular simulations through multi-level
parallelism from laptops to supercomputers. *SoftwareX*. **2015**, 1–2, 19–25.
42. Jorgensen, WL.; Chandrasekhar, J.; Madura, JD.; Impey, RW.; Klein, M.L.
Comparison of simple potential functions for simulating liquid water. *J. Chem. Phys.*
1983, 79, 6127-6129.
43. Best, RB.; Zhu, X.; Shim, J.; Lopes, PEM.; Mittal, J.; Feig, M.; MacKerell, AD.
Optimization of the additive CHARMM All-atom protein force field targeting
improved sampling of the backbone ϕ , ψ and side-chain χ_1 and χ_2 dihedral Angles. *J.*
Chem. Theory Comput. **2012**, 8, 3257–3273.
44. MacKerell, AD; Bashford, D.; Bellott, MRL.; Evanseck, JD.; Field, MJ.; Fischer, S.;
Gao, J.; Guo, H.; Ha, S.; Joseph-McCarthy, D.; Kuchnir, L.; Kuczera, K.; Lau, FTK.;
Mattos, C.; Michnick. S.; Ngo, T.; Nguyen, DT.; Prodhom, B.; Reiher, WE.; Roux,
B.; Schlenkrich, M.; Smith, JC.; Stote, R.; Straub, J.; Watanabe, M.; Wiórkiewicz-
Kuczera, J.; Yin, D.; Karplus M. All-atom empirical potential for molecular modeling
and dynamics studies of proteins. *J. Phys. Chem. B*. **1998**, 102, 3586-3616.
45. Darden, T.; York, D.; Pedersen L. Particle mesh Ewald: An Nlog(N) method for
Ewald sums in large systems. *J. Chem. Phys.* **1993**, 98, 10089-10092.
46. Towns, J.; Cockerill, T.; Dahan, M.; Foster, I.; Gaither, K.; Grimshaw, A.;
Hazlewood, V.; Lathrop, S.; Lifka, D.; Peterson, G.; Roskies, R.; Scott, JR.; Wilkins-
Diehr, N. XSEDE: Accelerating Scientific Discovery. *Computing in Science &*
Engineering. **2014**, 16 (5), 62-74.

47. Reiher, WH. Theoretical studies of hydrogen bonding; Harvard University:
Massachusetts, U.S.A., **1985**.

APPENDIX A

Interaction energies of interface residues of all predicted models show high interaction energies for charged residues¹

Residue ID	I.E.	Residue ID	I.E.	Residue ID	I.E.
MCE3-T176O	-2	MCE3-N61A	-2	MCE7-T62A	-5
MCE3-T177O	2	MCE3-T62A	2	MCE7-D63A	-40
MCE3-V178O	-6	MCE3-D63A	-4	MCE7-N67A	0
MCE3-R197O	-166	MCE3-G64A	-96	MCE7-Q69A	-9
MCE3-N205O	-33	MCE3-G64A	-1	MCE7-E70A	-47
MCE3-I206O	1	MCE3-A65A	-6	MCE7-W88C	-5
MCE3-P208O	-9	MCE3-H91C	-13	MCE7-E92C	-75
MCE3-F233O	-7	MCE3-E92C	-245	MCE9-V178O	-2
MCE3-V235O	-4	MCE7-V178O	-3	MCE9-I206O	-4
MCE3-T237O	0	MCE7-L203O	-3	MCE9-V235O	-4
MCE3-V242O	-3	MCE7-Q204O	-2	MCE9-T237O	-7
MCE3-D244O	91	MCE7-N205O	-4	MCE9-V242O	-2
MCE3-T246O	-18	MCE7-I206O	-11	MCE9-H279O	1
MCE3-Q280O	0	MCE7-P208O	-4	MCE9-Q280O	-28
MCE3-V281O	3	MCE7-F233O	-8	MCE9-V281O	0
MCE3-V282O	-4	MCE7-V235O	-5	MCE9-V282O	-7
MCE3-S283O	-5	MCE7-P236O	-2	MCE9-S283O	-5
MCE3-D296O	22	MCE7-T237O	-24	MCE9-S284O	-2
MCE3-G298O	0	MCE7-A238O	-19	MCE9-D296O	80
MCE3-A299O	-3	MCE7-V242O	0	MCE9-G298O	1
MCE3-G300O	-4	MCE7-H279O	2	MCE9-A299O	1
MCE3-I301O	-3	MCE7-Q280O	-4	MCE9-I301O	-5
MCE3-L303O	-13	MCE7-V281O	-1	MCE9-L303O	-10
MCE3-F307O	-6	MCE7-V282O	-6	MCE9-K309O	-102
MCE3-K309O	-165	MCE7-S283O	-11	MCE9-I311O	-3
MCE3-I311O	-3	MCE7-G298O	-5	MCE9-W313O	-6
MCE3-W313O	-4	MCE7-A299O	-6	MCE9-K84A	0
MCE3-H17A	2	MCE7-G300O	-1	MCE9-K85A	11
MCE3-L21A	0	MCE7-I301O	0	MCE9-H87A	-47
MCE3-I22A	4	MCE7-I311O	-3	MCE9-Q21C	-4
MCE3-K23A	-50	MCE7-W313O	-4	MCE9-V24C	-3
MCE3-N25A	-16	MCE7-L21A	-1	MCE9-K25C	18
MCE3-F26A	-17	MCE7-K23A	-4	MCE9-L26C	-4
MCE3-H27A	-9	MCE7-G24A	-4	MCE9-G27C	-10
MCE3-A28A	-11	MCE7-N25A	-4	MCE9-H28C	-25

Residue ID	I.E.	Residue ID	I.E.	Residue ID	I.E.
MCE3-Y30A	0	MCE7-F26A	-10	MCE9-P29C	-8
MCE3-R31A	-8	MCE7-H27A	-11	MCE9-D30C	-6
MCE3-D32A	-2	MCE7-Y30A	-2	MCE9-N33C	-4
MCE3-F55A	22	MCE7-N61A	-9	MCE9-N69C	0
MCE9-D71C	0	MCE15-F233O	-3	MCE21-H179O	-2
MCE9-Q73C	2	MCE15-V235O	-7	MCE21-A180O	3
MCE11-Y49O	-10	MCE15-P236O	-3	MCE21-I206O	0
				MCE21-	
MCE11-D50O	109	MCE15-T237O	-1	M231O	-2
MCE11-S51O	-6	MCE15-V242O	-1	MCE21-F233O	-6
MCE11-T52O	-3	MCE15-D244O	85	MCE21-V235O	-3
MCE11-H53O	2	MCE15-Q280O	-5	MCE21-T237O	-17
MCE11-G54O	-17	MCE15-V281O	-3	MCE21-V240O	-21
MCE11-K55O	-89	MCE15-V282O	-6	MCE21-S241O	-5
MCE11-L203O	-4	MCE15-S283O	-4	MCE21-V242O	-4
MCE11-I206O	-5	MCE15-G298O	-12	MCE21-D244O	2
MCE11-F233O	-1	MCE15-A299O	-3	MCE21-Q280O	-16
MCE11-P236O	3	MCE15-G300O	-10	MCE21-V281O	0
MCE11-V242O	-3	MCE15-I301O	-8	MCE21-V282O	-5
MCE11-D244O	84	MCE15-A302O	-4	MCE21-S283O	-8
MCE11-Q280O	-15	MCE15-L303O	-8	MCE21-G298O	1
MCE11-V281O	0	MCE15-K309O	-115	MCE21-A299O	-5
MCE11-V282O	-5	MCE15-W313O	-5	MCE21-G300O	-2
MCE11-V53A	-1	MCE15-I22A	-4	MCE21-I301O	-10
MCE11-K56A	42	MCE15-K23A	-50	MCE21-A302O	1
MCE11-E57A	-36	MCE15-G24A	-6	MCE21-L303O	-6
MCE11-I60A	-8	MCE15-N25A	-1	MCE21-N304O	-20
MCE11-N61A	-20	MCE15-F26A	-6	MCE21-F307O	-3
MCE11-T62A	-16	MCE15-H27A	2	MCE21-K309O	-12
MCE11-D63A	-2	MCE15-Y30A	-6	MCE21-I311O	-1
				MCE21-	
MCE11-Q69A	-13	MCE15-R31A	-53	W313O	-4
MCE11-E70A	1	MCE15-D32A	37	MCE21-M1A	-12
MCE11-K77A	25	MCE15-D33A	15	MCE21-L2A	-3
MCE11-K84A	28	MCE15-K35A	-4	MCE21-E4A	-38
MCE11-D67C	-61	MCE15-K36A	-30	MCE21-K7A	19
MCE11-T68C	-8	MCE15-F55A	-2	MCE21-S11A	1
MCE11-N69C	-6	MCE15-D59A	-12	MCE21-D14A	8
MCE11-A70C	-5	MCE15-N61A	1	MCE21-K18A	-53

Residue ID	I.E.	Residue ID	I.E.	Residue ID	I.E.
MCE11-M81C	1	MCE15-T62A	-8	MCE21-Y19A	-3
MCE11-R85C	-35	MCE15-D63A	-41	MCE21-T40A	-4
MCE11-W88C	-5	MCE15-G64A	0	MCE21-E41A	32
MCE11-E92C	10	MCE21-T176O	-4	MCE21-M1C	24
MCE15-V178O	-5	MCE21-T177O	0	MCE21-T2C	-12
MCE15-I206O	-2	MCE21-V178O	-10	MCE21-C3C	-2
MCE21-K4C	-61	DCE4-H27A	-1	DCE7-H17A	1
MCE21-M5C	1	DCE4-Q46C	-5	DCE7-L21A	-3
MCE21-S6C	-7	DCE4-N47C	-1	DCE7-I22A	-11
MCE21-Q7C	-2	DCE4-F48C	-27	DCE7-K23A	66
MCE21-R10C	-41	DCE4-L49C	2	DCE7-G24A	-3
MCE21-E13C	-23	DCE4-K50C	-108	DCE7-N25A	-4
DCE4-K3O	-261	DCE4-K51C	64	DCE7-F26A	-8
DCE4-V4O	10	DCE4-E52C	-121	DCE7-H27A	-11
DCE4-K5O	-51	DCE4-K54C	-50	DCE7-D32A	-75
DCE4-A22O	3	DCE4-A89C	-4	DCE7-N61A	8
DCE4-F23O	-2	DCE4-S90C	-4	DCE7-D63A	-206
DCE4-N24O	7	DCE4-H91C	-7	DCE7-A65A	-4
DCE4-S25O	-9	DCE4-E92C	-203	DCE7-Q69A	-4
DCE4-G26O	-4	DCE7-Y255O	-5	DCE7-K51C	-52
DCE4-K27O	-46	DCE7-D256O	40	DCE7-N55C	2
DCE4-D29O	82	DCE7-K259O	-67	DCE7-V58C	-1
DCE4-H57O	-2	DCE7-Q280O	-8	DCE7-R85C	-1
DCE4-G58O	-10	DCE7-G298O	1	DCE7-W88C	-30
DCE4-I69O	2	DCE7-G300O	0	DCE7-A89C	-8
DCE4-N70O	-19	DCE7-I301O	-3	DCE7-H91C	-20
DCE4-G71O	0	DCE7-E79P	-52	DCE7-E92C	-363
DCE4-N72O	-18	DCE7-R80P	-5	DCE9-M105O	-5
DCE4-E93O	-155	DCE7-D81P	-2	DCE9-A126O	0
DCE4-Y94O	-8	DCE7-K84P	-33	DCE9-D127O	94
DCE4-H137O	0	DCE7-G100P	11	DCE9-A128O	-1
DCE4-E138O	-17	DCE7-V101P	7	DCE9-P129O	-7
DCE4-D326O	22	DCE7-T103P	-26	DCE9-M130O	-3
DCE4-A329O	-2	DCE7-T104P	-2	DCE9-F131O	-2
DCE4-H330O	-23	DCE7-E106P	64	DCE9-N136O	-3
DCE4-M331O	-4	DCE7-K107P	-200	DCE9-K139O	-98
DCE4-A332O	-9	DCE7-A126P	-6	DCE9-Y140O	-3
DCE4-S333O	-23	DCE7-K194P	-246	DCE9-D141O	43
DCE4-K334O	15	DCE7-L195P	-7	DCE9-S143O	5

Residue ID	I.E.	Residue ID	I.E.	Residue ID	I.E.
DCE4-E335O	-134	DCE7-R197P	-63	DCE9-L144O	-5
DCE4-L2A	1	DCE7-S210P	-9	DCE9-G218O	0
DCE4-N10A	-3	DCE7-T211P	-1	DCE9-K219O	-107
DCE4-I13A	0	DCE7-G212P	-1	DCE9-V220O	-1
DCE4-H17A	0	DCE7-K215P	-184	DCE9-P222O	-4
DCE4-F26A	0	DCE7-K219P	-118	DCE9-N225O	-12
DCE9-K254P	16	DCE11-F26A	-2	TCE3-N67A	6
DCE9-M1A	66	DCE11-S90C	-8	TCE3-Q69A	-3
DCE9-L2A	1	DCE11-H91C	-10	TCE3-E70A	-140
DCE9-D14A	-93	DCE11-E92C	-288	TCE4-K3Q	-295
DCE9-H17A	-10	TCE3-D141P	6	TCE4-S25Q	3
DCE9-L21A	-21	TCE3-K334P	-48	TCE4-K27Q	-78
DCE9-I22A	-9	TCE3-E138P	47	TCE4-M133Q	-5
DCE9-K23A	24	TCE3-K139P	-231	TCE4-G134Q	-3
DCE9-G24A	-22	TCE3-Y140P	-5	TCE4-H137Q	-6
DCE9-N25A	-8	TCE3-S143P	-11	TCE4-E138Q	71
DCE9-F26A	-10	TCE3-L144P	-5	TCE4-G268Q	0
DCE9-H27A	-7	TCE3-P129P	-13	TCE4-P269Q	-1
DCE9-Y30A	-9	TCE3-K219P	-110	TCE4-L270Q	-2
DCE11-S192O	-22	TCE3-N225P	-9	TCE4-K271Q	-21
DCE11-G193P	-18	TCE3-G218P	3	TCE4-G272Q	-4
DCE11-K194O	-168	TCE3-M130P	-2	TCE4-I273Q	-5
DCE11-L195O	-4	TCE3-V220P	2	TCE4-D326Q	50
DCE11-W196O	-18	TCE3-P222P	-10	TCE4-A329Q	-5
DCE11-S210O	1	TCE3-I221P	-2	TCE4-H330Q	-10
DCE11-K215O	-120	TCE3-A128P	3	TCE4-M331Q	1
DCE11-K254P	-30	TCE3-F131P	-2	TCE4-A332Q	1
DCE11-Y255P	-12	TCE3-D127P	23	TCE4-S333Q	-5
DCE11-D256P	57	TCE3-N136P	-21	TCE4-K334Q	-104
DCE11-K259P	-87	TCE3-E223P	132	TCE4-18LYSA	84
DCE11-A297P	0	TCE3-K23A	45	TCE4-21LEUA	-4
DCE11-G298P	-2	TCE3-G24A	-1	TCE4-22ILEA	-5
DCE11-A299P	1	TCE3-N25A	1	TCE4-23LYSA	116
DCE11-G300P	2	TCE3-A28A	3	TCE4-24GLYA	-6
DCE11-I301P	-5	TCE3-Y30A	-15	TCE4-25ASNA	-20
DCE11-A302P	0	TCE3-R31A	43	TCE4-26PHEA	-18
DCE11-N10A	-4	TCE3-D32A	-46	TCE4-27HISA	-18
DCE11-I13A	-1	TCE3-F55A	-3	TCE4-30TYRA	-6
DCE11-H27A	60	TCE3-D59A	-129	TCE4-63ASPA	-180

Residue ID	I.E.	Residue ID	I.E.	Residue ID	I.E.
DCE11-Y30A	-15	TCE3-I60A	-6	TCE4-64GLYA	-6
DCE11-K18A	-8	TCE3-N61A	-14	TCE4-65ALAA	-1
DCE11-L21A	81	TCE3-T62A	-19	TCE7-D127O	21
DCE11-G24A	0	TCE3-D63A	-220	TCE7-A128O	3
DCE11-I22A	-10	TCE3-G64A	3	TCE7-P129O	-14
DCE11-K23A	-6	TCE3-A65A	-21	TCE7-M130O	-5
TCE7-F131O	-3	TCE9-K162P	-94	TCE9-S6C	-5
TCE7-N136O	-22	TCE9-H165P	0	TCE9-Q7C	-10
TCE7-E138O	50	TCE9-D166P	76	TCE9-L8C	0
TCE7-K139O	-216	TCE9-N167P	1	TCE9-R10C	73
TCE7-Y140O	-6	TCE9-F168P	0	TCE10-D127P	9
TCE7-D141O	5	TCE9-V220P	2	TCE10-A128P	0
TCE7-S143O	-10	TCE9-I221P	-4	TCE10-P129P	0
TCE7-L144O	-5	TCE9-P222P	-3	TCE10-M130P	0
TCE7-G218O	3	TCE9-E223P	71	TCE10-F131P	0
TCE7-K219O	-104	TCE9-K251P	-151	TCE10-N136P	0
TCE7-V220O	1	TCE9-P252P	1	TCE10-E138P	7
TCE7-I221O	-2	TCE9-K254P	2	TCE10-K139P	-8
TCE7-P222O	-11	TCE9-D257P	-28	TCE10-Y140P	0
TCE7-E223O	129	TCE9-K260P	-1	TCE10-D141P	8
TCE7-N225O	-6	TCE9-V261P	-6	TCE10-S143P	0
TCE7-K334O	-50	TCE9-Q264P	-22	TCE10-L144P	0
TCE7-K23A	43	TCE9-G268P	-7	TCE10-G218P	0
TCE7-G24A	-2	TCE9-P269P	-8	TCE10-K219P	-8
TCE7-N25A	4	TCE9-L2A	-2	TCE10-V220P	0
TCE7-A28A	1	TCE9-K7A	29	TCE10-I221P	0
TCE7-Y30A	-16	TCE9-N10A	-3	TCE10-P222P	0
TCE7-R31A	39	TCE9-S11A	-1	TCE10-E223P	7
TCE7-D32A	-47	TCE9-I13A	3	TCE10-N225P	0
TCE7-F55A	-5	TCE9-D14A	-115	TCE10-K334P	-7
TCE7-D59A	-126	TCE9-V15A	-2	TCE10-K23A	36
TCE7-I60A	-8	TCE9-H17A	-10	TCE10-G24A	0
TCE7-N61A	-10	TCE9-K18A	61	TCE10-N25A	0
TCE7-T62A	-19	TCE9-Y19A	-8	TCE10-A28A	0
TCE7-D63A	-218	TCE9-L21A	-10	TCE10-Y30A	0
TCE7-G64A	4	TCE9-I22A	-16	TCE10-R31A	35
TCE7-A65A	-11	TCE9-K23A	70	TCE10-D32A	-35
TCE7-N67A	8	TCE9-G24A	-8	TCE10-F55A	0
TCE7-Q69A	-5	TCE9-F26A	-4	TCE10-D59A	-36

Residue ID	I.E.	Residue ID	I.E.	Residue ID	I.E.
TCE7-E70A	-129	TCE9-D32A	-65	TCE10-I60A	0
TCE7-E92C	-139	TCE9-D33A	-80	TCE10-N61A	0
TCE9-V135P	4	TCE9-K36A	32	TCE10-T62A	0
TCE9-N136P	-4	TCE9-T40A	-6	TCE10-D63A	-37
TCE9-E138P	-22	TCE9-C3C	-3	TCE10-G64A	0
TCE9-K139P	-73	TCE9-M5C	-6	TCE10-A65A	0
TCE10-N67A	0	TCE15-P129P	0	TCE18-I273P	-4
TCE10-Q69A	0	TCE15-M130P	0	TCE18-D326P	47
TCE10-E70A	-38	TCE15-F131P	0	TCE18-A329P	-3
TCE10-E92C	-90	TCE15-N136P	0	TCE18-H330P	-8
TCE12-T59P	-10	TCE15-K139P	-8	TCE18-M331P	1
TCE12-K61P	-112	TCE15-D127P	9	TCE18-A332P	2
TCE12-A62P	0	TCE15-A128P	0	TCE18-S333P	-6
TCE12-E63P	75	TCE15-L144P	0	TCE18-K334P	-117
TCE12-N64P	-21	TCE15-Y140P	0	TCE18-K18A	84
TCE12-V68P	-4	TCE15-D141P	8	TCE18-L21A	-3
TCE12-N70P	-6	TCE15-S143P	0	TCE18-I22A	-3
TCE12-G71P	-3	TCE15-E250P	8	TCE18-K23A	135
TCE12-N72P	-3	TCE15-K251P	-7	TCE18-G24A	-5
TCE12-P73P	-5	TCE15-P252P	0	TCE18-N25A	-16
TCE12-K263R	0	TCE15-H306P	0	TCE18-F26A	-16
TCE12-E267R	-38	TCE15-I60A	0	TCE18-H27A	-22
TCE12-K271R	-40	TCE15-N61A	0	TCE18-Y30A	-4
TCE12-Y276R	-2	TCE15-T62A	0	TCE18-T62A	-7
TCE12-H291R	2	TCE15-D63A	-37	TCE18-D63A	-157
TCE12-T40A	-12	TCE15-G64A	0	TCE18-G64A	-4
TCE12-S86A	-10	TCE15-A65A	0	TCE18-A65A	-1
TCE12-H87A	-131	TCE15-N67A	0	TCE19-G193O	0
TCE12-C3C	5	TCE15-Q69A	0	TCE19-K194O	-157
TCE12-K4C	82	TCE15-H61C	0	TCE19-L195O	-11
TCE12-M5C	7	TCE15-D65C	-48	TCE19-W196O	-8
TCE12-S6C	4	TCE15-L66C	0	TCE19-R197O	-79
TCE12-Q7C	-2	TCE15-R85C	45	TCE19-S210O	-6
TCE12-E9C	-141	TCE18-K3P	-262	TCE19-K215O	-39
TCE12-R10C	47	TCE18-S25P	0	TCE19-T229O	-3
TCE12-N17C	-16	TCE18-K27P	-54	TCE19-Y255P	-7
TCE12-H20C	-12	TCE18-M133P	-7	TCE19-D256P	98
TCE12-Q21C	-9	TCE18-G134P	-2	TCE19-K259P	-117
TCE12-Y22C	-1	TCE18-H137P	-3	TCE19-K260P	-133

Residue ID	I.E.	Residue ID	I.E.	Residue ID	I.E.
TCE12-V24C	-9	TCE18-E138P	64	TCE19-E278P	97
TCE12-K25C	67	TCE18-G268P	1	TCE19-H279P	-27
TCE12-P29C	-3	TCE18-P269P	0	TCE19-Q280P	-16
TCE15-G218P	0	TCE18-L270P	-2	TCE19-A297P	-4
TCE15-K219P	-9	TCE18-K271P	-41	TCE19-G298P	-7
TCE15-P222P	0	TCE18-G272P	-2	TCE19-A299P	-2
TCE19-G300P	3	TCE20-E2500	-135	TCE20-K54C	-25
TCE19-I301P	-6	TCE20-K2510	13	MC1-R130	-127
TCE19-A302P	1	TCE20-P2520	-5	MC1-R160	-122
TCE19-D39R	93	TCE20-H3060	-4	MC1-F370	-1
TCE19-N41R	-14	TCE20-M105P	-3	MC1-Y420	-8
TCE19-Y42R	0	TCE20-S125P	2	MC1-Y450	-27
TCE19-A62R	-2	TCE20-A126P	2	MC1-M460	-7
TCE19-E63R	96	TCE20-D127P	49	MC1-Y490	1
TCE19-N64R	-24	TCE20-A128P	-1	MC1-D500	70
TCE19-G65R	-1	TCE20-P129P	-6	MC1-S510	-48
TCE19-D14A	-150	TCE20-V171P	3	MC1-T520	-9
TCE19-H17A	-19	TCE20-K219P	-110	MC1-I1810	-4
TCE19-K18A	94	TCE20-P222P	8	MC1-T1820	-5
TCE19-L21A	-6	TCE20-E223P	13	MC1-A1830	-5
TCE19-I22A	-1	TCE20-L224P	-3	MC1-Q1850	0
TCE19-K23A	176	TCE20-N225P	-8	MC1-K1860	-120
TCE19-G24A	5	TCE20-K227P	-88	MC1-T1870	-18
TCE19-N25A	-7	TCE20-R248P	2	MC1-V1880	-5
TCE19-F26A	-12	TCE20-L249P	-8	MC1-D1890	61
TCE19-H27A	-10	TCE20-E250P	-51	MC1-R2000	-98
TCE19-A28A	-1	TCE20-K251P	0	MC1-A2020	-5
TCE19-Y30A	0	TCE20-M1A	39	MC1-L2030	-9
TCE19-D32A	-173	TCE20-L2A	0	MC1-Q2040	-2
TCE19-N61A	-11	TCE20-E4A	-38	MC1-A2380	2
TCE19-T62A	-12	TCE20-K7A	-15	MC1-E3170	80
TCE19-D63A	-219	TCE20-N10A	0	MC1-N25A	-3
TCE19-G64A	-5	TCE20-I13A	-2	MC1-A28A	0
TCE19-N67A	4	TCE20-D14A	-140	MC1-Y30A	-6
TCE19-Q69A	-18	TCE20-H17A	-12	MC1-R31A	21
TCE19-E52C	-85	TCE20-K18A	89	MC1-F55A	-4
TCE19-I62C	-4	TCE20-L21A	-3	MC1-K56A	6
TCE19-D65C	-141	TCE20-I22A	-3	MC1-E57A	-35
TCE19-L66C	-1	TCE20-K23A	73	MC1-L58A	-3

Residue ID	I.E.	Residue ID	I.E.	Residue ID	I.E.
TCE19-L82C	-2	TCE20-G24A	-7	MC1-D59A	-87
TCE19-R85C	91	TCE20-N25A	-4	MC1-I60A	-8
TCE19-W88C	-12	TCE20-F26A	-7	MC1-N61A	-9
TCE19-H91C	-6	TCE20-N47C	-6	MC1-T62A	-27
TCE19-E92C	-315	TCE20-K50C	39	MC1-D63A	-100
TCE20-L249O	-5	TCE20-K51C	62	MC1-G64A	-9
MC1-A65A	-5	MC2-F55A	-4	MC3-A299O	-3
MC1-Q69A	-15	MC2-K56A	3	MC3-G300O	-5
MC1-E70A	-76	MC2-E57A	-36	MC3-I301O	-3
MC1-L72A	1	MC2-L58A	-3	MC3-L303O	-13
MC1-I73A	-2	MC2-D59A	-87	MC3-F307O	-6
MC1-I76A	0	MC2-I60A	-7	MC3-K309O	-173
MC1-K77A	32	MC2-N61A	-6	MC3-I311O	-4
MC1-M81C	-5	MC2-T62A	-24	MC3-W313O	-4
MC1-A84C	-2	MC2-D63A	-120	MC3-H17A	2
MC1-R85C	32	MC2-G64A	-8	MC3-L21A	0
MC2-R13O	-3	MC2-A65A	-5	MC3-I22A	3
MC2-R16O	-8	MC2-Q69A	-25	MC3-K23A	-55
MC2-F37O	-27	MC2-E70A	-77	MC3-G24A	-17
MC2-Y42O	2	MC2-L72A	1	MC3-N25A	-17
MC2-Y45O	-46	MC2-I73A	-2	MC3-F26A	-9
MC2-M46O	-9	MC2-I76A	0	MC3-H27A	-8
MC2-Y49O	-21	MC2-K77A	34	MC3-A28A	0
MC2-D50O	-4	MC2-M81C	-7	MC3-Y30A	-9
MC2-S51O	-4	MC2-A84C	-2	MC3-R31A	-4
MC2-T52O	3	MC2-R85C	21	MC3-D32A	25
MC2-I181O	-5	MC2-W88C	-2	MC3-F55A	-2
MC2-T182O	-130	MC3-T176O	-3	MC3-N61A	2
MC2-A183O	-2	MC3-T177O	2	MC3-T62A	-6
MC2-Q185O	83	MC3-V178O	-6	MC3-D63A	-91
MC2-K186O	-136	MC3-R197O	-154	MC3-G64A	-1
MC2-T187O	71	MC3-N205O	-35	MC3-A65A	-6
MC2-V188O	-9	MC3-I206O	3	MC3-H91C	-10
MC2-D189O	5	MC3-P208O	-10	MC3-E92C	-224
MC2-R200O	-7	MC3-F233O	-7	DC1-R13P	-123
MC2-A202O	-132	MC3-V235O	-3	DC1-R16P	-121
MC2-L203O	-6	MC3-T237O	0	DC1-F37P	-1
MC2-Q204O	56	MC3-V242O	-3	DC1-Y42P	-4
MC2-A238O	0	MC3-D244O	96	DC1-Y45P	-23

Residue ID	I.E.	Residue ID	I.E.	Residue ID	I.E.
MC2-E317O	-94	MC3-T246O	-17	DC1-M46P	-8
MC2-P191O	-1	MC3-V281O	1	DC1-Y49O	-28
MC2-N25A	-2	MC3-V282O	-6	DC1-Y49P	4
MC2-A28A	1	MC3-S283O	-4	DC1-D50O	55
MC2-Y30A	-6	MC3-D296O	19	DC1-D50P	68
MC2-R31A	25	MC3-G298O	-1	DC1-S51O	3
DC1-S51P	-46	DC1-K77A	50	DC2-S51P	-5
DC1-T52P	-11	DC1-L58A	-2	DC2-K55P	-127
DC1-K55O	-138	DC1-L72A	0	DC2-H57P	-24
DC1-H57O	-17	DC1-N25A	-2	DC2-G58P	3
DC1-I181P	-4	DC1-N61A	-7	DC2-S284P	4
DC1-T182P	-4	DC1-N69C	-7	DC2-D285P	117
DC1-A183P	-4	DC1-Q69A	-18	DC2-F286P	-1
DC1-Q185P	3	DC1-Q73C	-2	DC2-N287P	-1
DC1-K186P	-129	DC1-R31A	63	DC2-S288P	8
DC1-T187P	-23	DC1-T62A	-26	DC2-D289P	92
DC1-V188P	-6	DC1-T31C	-5	DC2-N25A	-9
DC1-A202P	-4	DC1-T68C	-4	DC2-A28A	1
DC1-L203P	-4	DC1-Y30A	-4	DC2-Y30A	-4
DC1-A238P	4	DC2-R13O	-135	DC2-R31A	53
DC1-S284O	1	DC2-R16O	-120	DC2-F55A	-3
DC1-D285O	115	DC2-F37O	-2	DC2-K56A	38
DC1-F286O	-2	DC2-Y42O	-1	DC2-E57A	-60
DC1-N287O	0	DC2-Y45O	-23	DC2-L58A	-2
DC1-S288O	7	DC2-M46O	-8	DC2-D59A	-108
DC1-D289O	108	DC2-Y49O	2	DC2-I60A	-5
DC1-E317P	78	DC2-D50O	78	DC2-N61A	-4
DC1-A28A	0	DC2-S51O	-49	DC2-T62A	-14
DC1-A65A	-5	DC2-T52O	-6	DC2-D63A	-117
DC1-D59A	-112	DC2-I181O	-2	DC2-G65A	-8
DC1-D63A	-120	DC2-T182O	-2	DC2-A65A	-6
DC1-D30C	-95	DC2-A183O	-1	DC2-Q69A	-13
DC1-D71C	-54	DC2-Q185O	4	DC2-E70A	-91
DC1-E57A	-56	DC2-K186O	-118	DC2-L72A	0
DC1-E70A	-92	DC2-T187O	-18	DC2-I73A	-3
DC1-E77C	-53	DC2-V188O	-7	DC2-I76A	-2
DC1-F55A	-3	DC2-A202O	57	DC2-K77A	54
DC1-G64A	-9	DC2-L203O	-95	DC2-K84A	52
DC1-H87A	-100	DC2-A238O	-4	DC2-H87A	-102

Residue ID	I.E.	Residue ID	I.E.	Residue ID	I.E.
DC1-H28C	-8	DC2-E317O	-8	DC2-H28C	-8
DC1-I60A	-6	DC2-D189O	-2	DC2-D30C	-98
DC1-I73A	-2	DC2-R200O	3	DC2-T31C	-10
DC1-I76A	-3	DC2-Q204O	94	DC2-T68C	-2
DC1-K84A	49	DC2-Y49P	-24	DC2-N69C	-4
DC1-K56A	30	DC2-D50P	42	DC2-D71C	-65
DC2-Q73C	-3	DC3-N25A	-11	TC1-H57P	-16
DC2-E77C	-68	DC3-A28A	0	TC1-G58P	-16
DC2-M81C	-8	DC3-Y30A	-4	TC1-T59P	-31
DC2-A84C	-3	DC3-R31A	50	TC1-K61P	-45
DC2-R85C	17	DC3-F55A	-3	TC1-N70P	-9
DC3-R13O	-136	DC3-K56A	37	TC1-G71P	-5
DC3-R16O	-122	DC3-E57A	-57	TC1-S288P	2
DC3-F37O	-2	DC3-L58A	-2	TC1-T290P	-13
DC3-Y42O	-3	DC3-D59A	-102	TC1-F318P	-5
DC3-Y45O	-23	DC3-I60A	-6	TC1-N322P	-2
DC3-M46O	-6	DC3-N61A	-6	TC1-N24R	2
DC3-Y49O	-3	DC3-T62A	-20	TC1-K55R	-78
DC3-D50O	77	DC3-D63A	-104	TC1-F56R	-3
DC3-S51O	-38	DC3-G64A	-10	TC1-H57R	-24
DC3-T52O	-6	DC3-A65A	-5	TC1-G58R	-9
DC3-I181O	-3	DC3-Q69A	-11	TC1-T59R	1
DC3-T182O	-2	DC3-E70A	-89	TC1-N70R	-8
DC3-A183O	-1	DC3-L72A	0	TC1-G71R	-4
DC3-Q185O	3	DC3-I73A	-2	TC1-E267R	-27
DC3-K186O	-118	DC3-I76A	-2	TC1-G268R	15
DC3-T187O	-19	DC3-K77A	50	TC1-L2A	3
DC3-V188O	-7	DC3-K84A	48	TC1-N10A	5
DC3-D189O	58	DC3-H87A	-93	TC1-D14A	-185
DC3-R200O	-96	DC3-H28C	-4	TC1-Y16A	2
DC3-A202O	-4	DC3-D30C	-101	TC1-H17A	-5
DC3-L203O	-9	DC3-T31C	-4	TC1-K18A	101
DC3-Q204O	-5	DC3-T68C	-5	TC1-Y19A	-2
DC3-A238O	2	DC3-N69C	-2	TC1-S20A	-1
DC3-E317O	95	DC3-D71C	-66	TC1-L21A	-10
DC3-Y49P	-21	DC3-Q73C	-5	TC1-I22A	-10
DC3-S51P	-4	DC3-M81C	-9	TC1-K23A	137
DC3-K55P	-141	DC3-A84C	-3	TC1-G24A	2
DC3-H57P	-16	DC3-R85C	20	TC1-N25A	-9

Residue ID	I.E.	Residue ID	I.E.	Residue ID	I.E.
DC3-G58P	3	TC1-R20P	-62	TC1-F26A	-9
DC3-S284P	5	TC1-F23P	-4	TC1-H27A	-3
DC3-D285P	115	TC1-N24P	-3	TC1-A28A	-2
DC3-F286P	-3	TC1-S25P	-5	TC1-V29A	-1
DC3-N287P	-6	TC1-H53P	2	TC1-Y30A	-1
DC3-S288P	1	TC1-F56P	2	TC1-N61A	-3
TC1-T62A	-9	TC2-Q78P	-13	TC1-Q69A	0
TC1-D63A	-154	TC2-E79P	94	TC1-Q7GC	-1
TC1-G64A	-2	TC2-K84P	-91	TC1-K51C	88
TC1-A65A	-6	TC2-I85P	-2	TC2-L40P	-7
TC1-V66A	-1	TC2-K86P	-205	TC2-N64P	-37
TC2-H20C	-19	TC2-D89P	97	TC2-G65P	-5
TC2-Q21C	-11	TC2-A90P	-3	TC2-K66P	-82
TC2-V24C	-6	TC2-T75P	-8	TC2-P29C	-9
TC2-K25C	78	TC2-I76P	-3	TC2-D30C	-150
TC2-L26C	-9	TC2-F77P	-11	TC2-E39C	-99
TC2-G27C	-11	TC2-H87A	-102	TC2-K43C	67

¹ Residue ID are defined as name of the candidate model followed by the interface residue on its respective chain. I.E. is the interaction energy of that residue with its binding subunit.

APPENDIX B

Virtual alanine scanning of all predicted models shows similar pattern to interaction energies. ^k

MCE3				MCE7			
S100A8A9	$\Delta\Delta G$	GAPDH	$\Delta\Delta G$	S100A8A9	$\Delta\Delta G$	GAPDH	$\Delta\Delta G$
H17A	0.04	T176	0.77	L21A	0.49	V178O	1.14
L21A	0.24	T177	5.07	K23A	1.36	L203O	0.56
I22A	0.15	V178	1.41	N25A	0.91	Q204O	-0.25
K23A	2.37	I206	1.58	F26A	1.03	N205O	-0.19
N25A	-0.30	F233	2.12	H27A	0.58	I206O	1.77
F26A	2.31	V235	2.25	Y30A	0.13	F233O	1.62
H27A	1.19	T237	0.62	I60A	0.23	V235O	1.80
Y30A	4.53	V242	2.57	N61A	-0.14	T237O	0.37
R31A	-0.23	D244	6.26	T62A	0.67	V242O	2.15
D32A	1.50	T246	4.42	D63A	0.53	H279O	-1.09
F55A	0.43	Q280	-1.10	Q69A	0.04	Q280O	-1.03
N61A	0.38	V281	1.03	E70A	-0.30	V281O	1.04
T62A	0.91	V282	0.86	W88C	1.10	V282O	1.14
D63A	0.93	S283	-0.58	E92C	-0.47	S283O	-0.55
H91C	0.30	D296	3.47			I311O	2.41
E92C	-0.21	I301	0.64			W313O	8.68
		L303	1.10	MCE11			
		F307	1.89	V53A	0.24	Y49O	2.08
		K309	5.68	K56A	-0.59	D50O	2.38
		I311	2.81	I60A	0.89	S51O	-0.56
		W313	9.80	N61A	1.14	T52O	0.67
MCE15				T62A	0.37	H53O	3.91
I22A	0.19	V282O	0.46	D63A	0.53	L203O	0.16
K23A	3.79	W313O	8.36	Q69A	0.46	I206O	2.08
N25A	0.72	V281O	0.91	E70A	0.49	F233O	0.91
F26A	2.47	V178O	1.28	K77A	0.03	V242O	2.34
H27A	-0.12	V242O	2.23	K84A	-0.11	D244O	0.95
Y30A	0.66	V235O	2.58	D67C	-0.07	Q280O	-0.31
R31A	0.34	F233O	1.54	T68C	0.04	V281O	0.95
D32A	2.97	I206O	1.58	N69C	0.64	V282O	1.17
D33A	1.13	T237O	0.72	A70C	-0.04	S284O	-0.23
K35A	0.17	Q280O	-0.62	M81C	0.18	I301O	0.26
K36A	-0.15	I301O	0.13	R85C	-0.10	K309O	3.44
F55A	0.29	L303O	0.71	W88C	0.79	I311O	2.94
D59A	-0.33	K309O	3.13	E92C	-0.02	W313O	8.33
D63A	0.55						

DC3				TC-1			
S100A8A9	$\Delta\Delta G$	GAPDH	$\Delta\Delta G$	S100A8A9	$\Delta\Delta G$	GAPDH	$\Delta\Delta G$
N25A	0.75	R13O	8.52	H17A	-0.62	K61P	-1.11
Y30A	0.78	R16O	3.22	K51C	-0.11	N24P	-0.70
R31A	-0.12	F37O	-0.01	L2A	-0.04	N24R	-0.33
F55A	0.17	Y42O	1.82	N10A	-0.03	N322P	-0.31
K56A	-0.04	Y45O	2.58	K23A	-0.02	K55R	-0.19
E57A	0.04	M46O	0.99	N67A	0.02	E267R	-0.10
L58A	0.05	Y49O	1.37	Y16A	0.04	S25P	0.17
D59A	1.24	D50O	5.12	Q69A	0.08	H57R	0.31
I60A	1.42	S51O	0.85	Y30A	0.14	S288P	0.56
N61A	0.38	T52O	0.46	D63A	0.19	T59R	0.63
T62A	0.57	I181O	1.74	Q7C	0.19	H57P	0.77
D63A	0.49	T182O	3.75	Y19A	0.21	T290P	1.27
Q69A	0.36	A183O	0	N61A	0.23	N70R	1.31
E70A	-0.13	Q185O	4.79	H27A	0.37	N70P	2.16
L72A	0.18	K186O	0.34	K18A	0.44	T59P	2.17
I73A	0.66	T187O	0.02	I22A	0.47	H53P	2.49
I76A	0.31	V188O	1.72	T62A	0.92	F318P	2.63
K77A	-0.29	D189O	1.09	N25A	1.01	F23P	3.26
K84A	0.46	R200O	3.16	L21A	1.25	F56R	3.31
H87A	0.1	L203O	0.68	F26A	1.80	F56P	3.76
H28C	0.33	Q204O	-0.31	D14A	2.74	R20P	3.80
D30C	-0.12	E317O	5.78	TC2			
T31C	0.04	Y49P	2.06	V24C	0.83	L40P	3.04
T68C	-0.02	S51P	-0.2	K25C	1.51	N64P	0.83
N69C	0.67	K55P	-0.44	L26C	1.88	K66P	1.32
D71C	0.59	H57P	0.34	H28C	0.71	I74P	4.11
Q73C	0.14	S284P	-0.28	E39C	1.75	T75P	1.55
M81C	0.27	D285P	1.73	K43C	-0.01	I76P	3.53
R85C	0.15	F286P	2.86			F77P	4.77
		N287P	-0.14			Q78P	1.56
		S288P	0.41			E79P	0.27
						K84P	-0.36
						I85P	2.63
						K86P	-0.68
						D89P	-1.38

DCE4				DCE7			
S100A8A9	$\Delta\Delta G$	GAPDH	$\Delta\Delta G$	S100A8A9	$\Delta\Delta G$	GAPDH	$\Delta\Delta G$
M1A	0.44	K3O	0.33	H17A	0.49	Y255O	3.01
L2A	0.70	V4O	1.85	L21A	0.57	D256O	-1.08
N10A	0.32	K5O	-0.49	I22A	-0.11	K259O	1.34
I13A	0.31	F23O	3.54	K23A	1.35	Q280O	0.50
H17A	0.13	N24O	-0.23	N25A	0.74	I301O	1.65
F26A	0.20	S25O	0.24	F26A	1.96	E79P	0.21
H27A	0.17	K27O	0.51	H27A	0.48	R80P	0.24
Q46C	0.45	D29O	-1.27	D32A	1.57	D81P	0.51
N47C	3.17	H57O	0.14	N61A	0.31	K84P	-0.61
F48C	0.11	I69O	3.84	D63A	0.41	V101P	0.75
K50C	-0.70	N70O	2.70	Q69A	-0.25	T103P	1.50
K51C	-0.50	N72O	0.39	K51C	-0.78	T104P	0.37
E52C	-0.12	E93O	0.30	N55C	-0.04	E106P	-0.46
K54C	-0.13	Y94O	3.64	V58C	-0.02	K107P	-0.47
S90C	0.27	H137O	2.10	W88C	0.32	K194P	2.12
H91C	0.12	E138O	-0.10	H91C	0.18	L195P	2.06
E92C	-0.11	D326O	0.41	E92C	1.07	R197P	7.59
		H330O	1.45			S210P	-0.18
		M331O	1.74			T211P	1.92
		S333O	0.10			K215P	-0.73
		K334O	0.39			K219P	-0.19
		E335O	-3.30				
DCE-9				DCE11			
M1A	-0.26	M105O	0.81	N10A	0.06	W196O	1.21
L2A	-0.02	D127O	0.51	I13A	0.31	L195O	0.70
D14A	-0.09	M130O	1.53	H27A	0.24	S210O	0.35
H17A	0.09	F131O	4.77	L21A	0.61	K215O	-0.66
L21A	1.11	N136O	3.96	I22A	0.12	K194O	1.03
I22A	0.02	K139O	0.38	K23A	1.11	S192O	-0.59
K23A	1.31	Y140O	4.16	F26A	2.22	D256P	-1.19
N25A	0.72	D141O	-0.11	H91C	0.37	K259P	0.91
F26A	3.39	S143O	0.60	E92C	-0.62	Y255P	3.36
H27A	0.42	L144O	2.78			K254P	-0.03
Y30A	0.31	K219O	0.17			A302P	0.01
		V220O	2.20			I301P	1.64
		K254P	-0.42				

TCE3				TCE7			
S100A8A9	$\Delta\Delta G$	GAPDH	$\Delta\Delta G$	S100A8A9	$\Delta\Delta G$	GAPDH	$\Delta\Delta G$
K23A	1.18	D141P	0.23	K23A	1.18	D127O	0.53
N25A	0.72	K334P	0.23	N25A	0.68	M130O	1.55
Y30A	1.60	E138P	-0.08	Y30A	1.40	F131O	4.59
R31A	-0.42	K139P	0.58	R31A	-0.82	N136O	3.77
D32A	1.47	Y140P	4.18	D32A	1.48	K139O	0.23
F55A	0.19	L144P	2.71	F55A	0.21	Y140O	4.16
D59A	0.34	K219P	0.17	D59A	-0.22	D141O	0.59
N61A	1.48	N225P	0.54	N61A	-0.26	S143O	-0.39
T62A	0.95	M130P	1.53	T62A	0.95	L144O	2.56
D63A	2.67	V220P	2.11	D63A	0.63	K219O	0.14
N67A	0.18	I221P	1.79	N67A	0.17	V220O	2.11
Q69A	0.28	F131P	4.55	Q69A	0.23	I221O	1.79
E70A	0.38	D127P	0.47	E70A	-0.12	E223O	-0.26
		N136P	4.80	E92C	-0.07	N225O	0.53
		E223P	-0.18			K334O	0.25
TCE9				TCE10			
L2A	0.19	V135P	2.52	K23A	1.19	D127P	0.48
K7A	-0.22	N136P	3.78	N25A	0.69	M130P	1.53
S11A	1.26	E138P	-0.14	Y30A	1.24	F131P	4.59
D14A	-0.69	K139P	-0.35	R31A	-0.82	N136P	3.76
H17A	0.68	K162P	2.12	D32A	1.48	E138P	-0.05
K18A	2.59	H165P	2.09	F55A	0.21	K139P	0.22
Y19A	0.41	D166P	-1.66	D59A	-0.22	Y140P	4.17
L21A	0.17	N167P	0.72	N61A	-0.30	D141P	0.58
I22A	0.51	F168P	3.50	T62A	0.70	S143P	-0.34
K23A	1.38	V220P	2.07	D63A	0.63	L144P	2.53
F26A	1.60	I221P	2.22	N67A	0.17	K219P	0.16
D32A	1.34	E223P	-1.03	Q69A	0.23	V220P	2.12
D33A	-0.10	K251P	0.23	E70A	-0.12	I221P	1.78
K36A	0.11	K254P	-0.15	E92C	-0.07	E223P	-0.26
T40A	0.22	D257P	-0.51			N225P	0.54
Q7C	4.40	K260P	-0.51			K334P	0.24
R10C	2.67	V261P	1.32				
		Q264P	2.12				

TCE12				TCE19			
S100A8A9	$\Delta\Delta G$	GAPDH	$\Delta\Delta G$	S100A8A9	$\Delta\Delta G$	GAPDH	$\Delta\Delta G$
H87A	0.13	T59P	1.30	D14A	-0.19	K194O	0.59
K4C	0.18	K61P	-2.12	H17A	0.99	L195O	1.16
E9C	-0.11	E63P	-1.35	L21A	0.63	W196O	2.80
N17C	-1.03	N64P	0.89	I22A	-0.02	R197O	7.05
Q21C	0.46	V68P	2.19	K23A	0.46	S210O	0.46
V24C	0.57	N70P	1.79	F26A	1.98	K215O	-1.55
K25C	-0.63	N72P	0.21	H27A	0.83	Y255P	2.32
		K263R	-0.21	Y30A	0.39	D256P	-1.26
		K271R	-1.28	D32A	1.09	K259P	1.81
		Y276R	3.41	N61A	0.51	K260P	-0.84
		H291R	0.29	T62A	-0.02	E278P	-0.64
TCE15				D63A	0.37	H279P	-0.26
I60A	0.70	M130P	1.44	Q69A	0.65	Q280P	0.99
N61A	2.30	F131P	4.37	E52C	-0.10	I301P	2.25
T62A	0.34	N136P	3.85	D65C	-0.16	D39R	0.35
D63A	0.80	K139P	-0.28	R85C	0.18	N41R	-0.64
Q69A	0.57	D127P	0.51	W88C	0.80	Y42R	4.00
H61C	1.02	L144P	2.87	E92C	-0.19	E63R	-0.53
D65C	-1.06	Y140P	4.16			N64R	0.56
L66C	-0.03	D141P	-0.10	TCE-20			
R85C	0.57	S143P	0.61	M1A	0.17	L249O	3.43
		E250P	-0.23	L2A	0.69	E250O	-0.53
		H306P	0.94	E4A	-0.08	K251O	-0.14
TCE18				K7A	-0.33	H306O	-0.10
K18A	0.04	K3P	1.14	N10A	0.47	M105P	1.21
L21A	0.25	S25P	0.19	I13A	0.18	S125P	1.10
I22A	0.32	K27P	0.1	D14A	-1.17	D127P	0.30
K23A	0.43	M133P	2.08	H17A	0.41	V171P	1.80
N25A	0.42	H137P	1.89	K18A	0.10	K219P	-0.06
F26A	1.83	E138P	0.54	L21A	0.54	E223P	-0.28
H27A	1.55	L270P	2.47	I22A	0.04	L224P	3.18
Y30A	0.79	K271P	0.37	K23A	0.02	N225P	0.80
D63A	0.56	I273P	2.39	N25A	0.57	K227P	1.03
		D326P	3.86	F26A	1.91	R248P	2.96
		H330P	2.19	N47C	-0.02	L249P	3.43
		M331P	1.75	K50C	0.25	E250P	-0.70
		K334P	0.61	K54C	0.74		

MC-1				MC3			
S100A8A9	$\Delta\Delta G$	GAPDH	$\Delta\Delta G$	S100A8A9	$\Delta\Delta G$	GAPDH	$\Delta\Delta G$
N25A	0.72	R13O	8.78	L21A	0.22	T176O	0.77
Y30A	0.39	R16O	3.22	I22A	0.13	T177O	5.07
R31A	-0.11	Y42O	1.50	K23A	2.43	V178O	1.44
F55A	0.20	Y45O	2.37	N25A	-0.31	R197O	0.27
K56A	0.11	M46O	1.02	F26A	2.26	N205O	-0.15
D59A	1.26	Y49O	1.38	H27A	1.15	I206O	1.58
I60A	1.46	D50O	5.12	Y30A	4.59	F233O	2.14
N61A	0.39	S51O	0.89	R31A	-0.23	V235O	2.21
T62A	0.99	T52O	0.46	D32A	1.02	T237O	0.61
D63A	0.49	I181O	1.69	F55A	0.46	V242O	2.66
Q69A	0.38	T182O	3.73	N61A	0.37	D244O	6.26
E70A	-0.14	Q185O	4.79	T62A	0.92	T246O	4.44
L72A	0.18	K186O	0.33	D63A	1.00	V281O	1.02
I73A	0.79	V188O	1.65	H91C	0.33	V282O	0.87
I76A	0.31	D189O	1.26	E92C	-0.19	S283O	-0.57
K77A	-0.24	R200O	1.25			D296O	3.47
M81C	0.29	L203O	0.68			I301O	0.78
R85C	0.25	E317O	5.81			L303O	1.15
MC2						F307O	1.93
N25A	0.76	R13O	8.49			K309O	5.74
Y30A	0.63	R16O	3.18			I311O	2.83
F55A	0.18	Y42O	1.61			W313O	9.79
D59A	1.17	Y45O	3.15				
I60A	1.53	Y49O	1.37				
N61A	0.41	D50O	5.13				
T62A	0.85	S51O	0.79				
D63A	0.52	T52O	0.54				
Q69A	0.37	I181O	1.72				
E70A	-0.15	T182O	3.75				
L72A	0.19	Q185O	4.8				
I73A	0.67	K186O	0.32				
I76A	0.33	V188O	1.71				
K77A	-0.28	D189O	1.34				
M81C	0.32	R200O	1.26				
W88C	0.28	E317O	5.99				

DC-1				DC2			
S100A8A9	$\Delta\Delta G$	GAPDH	$\Delta\Delta G$	S100A8A9	$\Delta\Delta G$	GAPDH	$\Delta\Delta G$
N25A	0.77	R13P	8.54	N25A	0.71	R13O	8.57
H28C	0.19	R16P	3.07	Y30A	0.86	R16O	3.2
D30C	-0.13	Y42P	1.95	R31A	-0.14	F37O	-0.02
Y30A	0.97	Y45P	2.53	F55A	0.15	Y42O	1.85
R31A	-0.13	Y49P	1.37	K56A	-0.05	Y45O	2.44
F55A	0.17	Y49O	1.83	E57A	0.04	M46O	1.01
K56A	-0.03	D50O	2.41	L58A	0.05	Y49O	1.36
E57A	0.03	D50P	5.24	D59A	1.43	D50O	5.12
L58A	0.05	T52P	0.44	I60A	1.35	S51O	1.02
D59A	0.41	K55O	-0.55	N61A	0.38	T52O	0.32
I60A	1.39	H57O	0.20	T62A	0.43	I181O	1.72
N61A	0.36	I181P	1.81	D63A	0.47	T182O	3.73
T62A	0.44	T182P	3.80	Q69A	0.38	Q185O	4.79
D63A	0.49	Q185P	4.89	E70A	-0.12	K186O	0.38
T68C	-0.05	K186P	0.47	L72A	0.2	T187O	0.06
Q69A	0.39	V188P	1.73	I73A	0.72	V188O	1.75
N69C	0.69	D189P	0.99	I76A	0.31	L203O	0.67
E70A	-0.12	R200P	2.92	K77A	-0.3	E317O	5.8
D71C	0.59	L203P	0.73	K84A	0.58	D189O	0.86
L72A	0.20	Q204P	-0.48	H87A	-0.08	R200O	3.15
Q73C	0.12	S284O	-0.25	H28C	0.28	Q204O	-0.44
I73A	0.73	D285O	1.46	D30C	0.88	Y49P	1.85
I76A	0.32	F286O	2.87	T31C	-0.09	D50P	2.45
K77A	-0.31	S288O	0.40	T68C	-0.03	S51P	-0.13
K84A	0.62	D289O	-0.23	N69C	1.55	K55P	-0.6
W88C	0.34	E317P	4.51	D71C	0.58	H57P	0.2
				Q73C	0.12	S284P	-0.29
				E77C	-0.09	D285P	1.72
				M81C	0.11	F286P	2.86
				R85C	-0.16	N287P	-0.13
						S288P	0.4
						D289P	-0.14

MCE15				MCE21			
S100A8A9	$\Delta\Delta G$	GAPDH	$\Delta\Delta G$	S100A8A9	$\Delta\Delta G$	GAPDH	$\Delta\Delta G$
I22A	0.19	V282O	0.46	M1A	0.29	T176O	0.51
K23A	3.79	W313O	8.36	L2A	0.33	T177O	5.07
N25A	0.72	V281O	0.91	E4A	-0.35	V178O	1.36
F26A	2.47	V178O	1.28	K7A	0.32	H179O	2.71
H27A	-0.12	V242O	2.23	S11A	1.23	I206O	1.07
Y30A	0.66	V235O	2.58	D14A	-0.08	M231O	0.93
R31A	0.34	F233O	1.54	K18A	1	F233O	2.07
D32A	2.97	I206O	1.58	Y19A	1.17	V235O	1.67
D33A	1.13	T237O	0.72	T40A	0.09	T237O	0.83
K35A	0.17	Q280O	-0.62	E41A	1.73	V240O	2.17
K36A	-0.15	I301O	0.13	M1C	0.53	S241O	3.53
F55A	0.29	L303O	0.71	T2C	-0.26	V242O	1.92
D59A	-0.33	K309O	3.13	C3C	-0.05	D244O	0.95
N61A	0.39	D244O	1.14	K4C	1.64	Q280O	-0.36
T62A	0.81			M5C	0.03	V281O	0.95
D63A	0.55			S6C	-0.04	V282O	1.05
				Q7C	2.32	S283O	-0.64
				R10C	-0.27	I301O	0.8
				E13C	-0.16	L303O	1.45
						N304O	0.43
						F307O	1.29
						K309O	2.76
						I311O	2.54
						W313O	8.97

^k $\Delta\Delta G$ is the change in binding energy upon virtual alanine scanning on the interface residues of S100A8A9 and GAPDH for a given predicted complex.